JoS JOURNAL OF STROKE

Journal of Stroke 2026;28(1):1-28
https://doi.org/10.5853/jos.2025.04168

Review

Multimodal Magnetic Resonance Imaging Signatures of White Matter Hyperintensities: Mechanistic Insights Into Pathobiological Heterogeneity

Jinyong Chung,[1,2,*] Hyerin Oh,[1,2,*] Dong-Seok Gwak,[2,3] Dong-Eog Kim[1,2,3]

[1]Medical Science Research Center, Dongguk University, Goyang, Korea
[2]National Priority Research Center for Stroke, Goyang, Korea
[3]Department of Neurology, Dongguk University Ilsan Hospital, Goyang, Korea

White matter hyperintensity (WMH), a common magnetic resonance imaging (MRI) marker of cerebral small-vessel disease, is associated with chronic cerebral ischemia; however, the mechanistic heterogeneity of WMH remains poorly defined. This review integrates multimodal MRI findings into a mechanism-oriented framework spanning four axes: WMH versus normal-appearing white matter (NAWM), periventricular versus deep location, lesion core versus perilesional penumbra, and longitudinal evolution. Periventricular WMHs are associated with blood–brain barrier dysfunction, interstitial fluid accumulation, and venous remodeling, whereas deep WMHs are more closely associated with impaired glymphatic/perivascular clearance and enlarged perivascular spaces, and demyelination/macromolecular compromise varying by context. The perilesional penumbra emerges as a critical transition zone, showing distance-dependent gradients of microstructural rarefaction, extracellular fluid expansion, perfusion deficits, and reduced vascular reactivity that extend beyond fluid-attenuated inversion recovery-defined borders and relate to subsequent lesion growth. Longitudinal data further indicate that abnormalities in diffusion, perfusion, and vascular reserve within NAWM precede new WMHs, nominating imaging biomarkers of progression risk. This framework supports risk stratification beyond total lesion burden, links therapeutic opportunities to mechanism (e.g., blood–brain barrier integrity, glymphatic clearance, and cerebrovascular reactivity), and motivates biologically interpretable readouts for patient selection and treatment monitoring. Looking forward, standardized spatial classification (including fine-grained, distance-informed parcellations), harmonized penumbra definitions, and integration of multimodal MRI with pathology will be essential to validate mechanism-specific subtypes and translate them into scalable, clinically usable endpoints.

Keywords White matter hyperintensity; Magnetic resonance imaging; Heterogeneity; Pathobiology; Spatial classification

Correspondence: Dong-Eog Kim
Department of Neurology, Dongguk University Ilsan Hospital, 27 Dongguk-ro, Ilsandong-gu, Goyang 10326, Korea
Tel: +82-31-961-7211
E-mail: kdongeog@duih.org
https://orcid.org/0000-0002-9339-6539

Received: August 26, 2025
Revised: December 14, 2025
Accepted: December 24, 2025

*These authors contributed equally as first author.

Introduction

White matter hyperintensities (WMHs) are highly prevalent magnetic resonance imaging (MRI) markers of brain aging and a core imaging feature of cerebral small-vessel disease (cSVD).[1-4] Although frequently asymptomatic in early stages,[5] increasing WMH burden[6] is progressively linked to cognitive decline,[7,8] dementia,[8,9] gait disturbance,[10,11] and higher mortality.[12,13] Of note,

Copyright © 2026 Korean Stroke Society
This is an Open Access article distributed under the terms of the Creative Commons Attribution Non-Commercial License (http://creativecommons.org/licenses/by-nc/4.0/) which permits unrestricted non-commercial use, distribution, and reproduction in any medium, provided the original work is properly cited.

WMH burden is also associated with increased stroke risk[12,13] and poorer stroke outcomes.[14,15] Yet, the mechanisms underlying WMH onset and progression remain incompletely understood, limiting precise risk stratification, longitudinal monitoring, and the development of targeted interventions.

A major challenge lies in the marked pathobiological heterogeneity of WMHs, which encompasses a spectrum of white matter injuries—including demyelination/axonal loss, hypoperfusion, blood–brain barrier (BBB) dysfunction, impaired glymphatic/perivascular clearance, ependymal disruption, as demonstrated in postmortem studies.[16-22] To conceptualize this diversity, two complementary frameworks are commonly applied. The first is a spatial framework: lesion location along the ventricle-to-cortex gradient (e.g., periventricular vs. deep) provides a mechanistic context.[3,23-25] The second extends beyond the visibly demarcated lesion, framing WMHs within a tissue continuum that incorporates the perilesional "penumbra" and surrounding normal-appearing white matter (NAWM),[26-28] where subtle structural and microvascular abnormalities often precede lesion formation and progression.[29-31] In this review, perilesional NAWM is used strictly as a spatial descriptor, referring to NAWM located adjacent to the lesion margin, whereas perilesional penumbra is an interpretive concept, denoting the subset of tissue within this spatial zone that is at risk and already exhibits subclinical abnormalities on advanced imaging.

Multimodal MRI has become indispensable for characterizing these heterogeneous pathobiological states *in vivo*.[18,32,33] By integrating quantitative contrasts probing microstructural damage (diffusion and water content), myelin and macromolecular integrity, BBB integrity and perfusion, and metabolic disturbances, advanced MRI approaches yield reproducible signatures that more directly link imaging phenotypes to underlying mechanisms—addressing key limitations of conventional lesion volume metrics.[32,34-38] Despite rapid advances in multimodal MRI research on WMH, no recent review has synthesized evidence in a manner that encompasses the following four key dimensions: WMH versus NAWM, periventricular versus deep WMH (PVWMH and DWMH, respectively), WMH core versus its penumbra, and longitudinal WMH progression. This review integrates multimodal MRI signatures into a concise, mechanism-oriented framework for understanding WMH heterogeneity and highlights these four contrasts as critical for clarifying the drivers of lesion progression. Accordingly, some degree of thematic overlap across sections is intentional, to allow each section to be read independently without requiring frequent cross-referencing.

Multimodal MRI signatures of WMH pathobiology

While conventional fluid-attenuated inversion recovery (FLAIR) imaging remains the reference standard for anatomically delineating WMH cores, it provides limited insight into the underlying tissue injury. Histopathologic studies have revealed that these hyperintense regions encompass diverse pathological processes—including demyelination and axonal loss, chronic hypoperfusion, BBB dysfunction, impaired glymphatic and perivascular clearance, and ependymal disruption—highlighting the heterogeneous nature of WMH.[16-22] This heterogeneity underscores the limitation of relying solely on intensity-based delineation, as simple T2-weighted or FLAIR hyperintensity cannot specify the underlying tissue alterations. To move beyond anatomical mapping toward mechanistic understanding, a range of advanced multimodal MRI techniques is required. This section, therefore, provides a concise overview of key imaging modalities used to probe the microstructural, vascular, and metabolic alterations of WMH—highlighting their utility in linking imaging phenotypes to underlying pathophysiologic mechanisms (Table 1)—as well as current methods for WMH delineation.

WMH delineation and spatial classification

As previously mentioned, conventional T2-weighted and FLAIR sequences remain the standard for WMH delineation (Figure 1A).[33,39-41] These contrasts are highly sensitive to increased tissue water: damaged white matter exhibits prolonged T2 relaxation, appearing hyperintense. FLAIR improves periventricular lesion detection by suppressing cerebrospinal fluid (CSF) signal. Accordingly, WMHs are defined as hyperintense regions identified through intensity-based methods on T2-weighted (including FLAIR) MRI, predominantly located in the periventricular and deep white matter.

Although WMHs were traditionally evaluated visually—with lesion burden often graded qualitatively using scales such as the Fazekas score, or delineated manually for volumetric estimation[24,42-44]—recent methodological advances have led to the widespread adoption of semi-automated and fully automated approaches, enabling more detailed and quantitative analyses.[45-47] A potential challenge arises in stroke patients when there is a delay between stroke onset and FLAIR acquisition: acute ischemic lesions, which appear hyperintense on diffusion-weighted imaging (DWI), may also exhibit hyperintensity on T2-weighted or FLAIR sequences, complicating their distinction from WMH.[48-50] In such instances, the typically symmetric distribution of WMH can assist in differentiation.[33,51,52] Nevertheless, caution is warranted, as asymmetric WMH patterns may occur and can them-

https://doi.org/10.5853/jos.2025.04168

Table 1. Multimodal MRI signatures of WMH pathobiology (vs. NAWM)

Study	Subjects	MRI features	Spatial classification	Main findings
Marstrand et al.[131] (2002)	Normal (n=21)	CBF, MTT	All WMH	Lower CBF and higher MTT in WMH.
Bastin et al.[67] (2009)	Non-demented normal (n=42)	FA, MD, AD, RD MTR	PVWMH (DWMH not examined)	Lower FA and MTR, and higher MD, AD, and RD in PVWMH.
Xing et al.[145] (2013)	Patients with WMH (n=45)	NAA/Cr, Cho/Cr	All WMH	Lower NAA/Cr and higher Cho/Cr in WMH.
Aradi et al.[144] (2013)	Migraine (n=17)	NAA, Cr	DWMH (no PVWMH cases)	Lower NAA and Cr in WMH.
Bernbaum et al.[132] (2015)	Minor stroke/TIA (n=40)	CBF	All WMH	Lower CBF in WMH.
Maniega et al.[27] (2015)	Population-based cohort (n=676)	R1 FA, MD MTR	All WMH	Lower R1, FA, and MTR, and higher MD in WMH.
Sun et al.[90] (2017)	Patients with WMH (n=32)	D, D*, f	PVWMH and DWMH	Higher D and f, and lower D* in both PVWMH and DWMH.
Wong et al.[87] (2017)	cSVD (n=73) and normal (n=40)	D, D*, f	All WMH	Higher D, D*, and f in WMH.
Jiaerken et al.[68] (2019)	Alzheimer's disease spectrum (n=40)	FA, MD FDG-PET rSUV	All WMH	Lower FA and FDG-PET rSUV, and higher MD in WMH.
Promjunyakul et al.[69] (2018)	Cognitively normal (n=52)	FA, MD, AD, RD CBF	PVWMH and DWMH	Lower CBF and FA, and higher MD, AD, and RD in both PVWMH and DWMH; differences less pronounced in DWMH.
Park et al.[119] (2019)	Cognitive complaints (n=99)	V_{MY}	PVWMH and DWMH	Lower V_{MY} in both PVWMH and DWMH.
Iordanishvili et al.[118] (2019)	Non-demented normal (n=70)	R1, R2*, H_2O MTR, f_{bound}	PVWMH and DWMH	Lower R1, R2*, MTR, and f_{bound}, and higher H_2O in both PVWMH and DWMH.
Wong et al.[182] (2019)	cSVD (n=27)	CBF V_L	All WMH	Lower CBF and higher V_L in WMH.
Khan et al.[55] (2020)	Stroke (n=97)	T_w, T_g, T_c	JVWMH, PVWMH, and DWMH	Lower T_w, and higher T_g and T_c in WMH.
Khan et al.[97] (2021)	Stroke (n=63)	T_w, T_g, T_c	All WMH	Lower T_w, and higher T_g and T_c in WMH.
Kerkhofs et al.[91] (2021)	cSVD (n=43)	K_i, V_L D	All WMH	Higher K_i, V_L, and D in WMH.
Etherton et al.[73] (2021)	Stroke (n=319)	AD, RD	All WMH	Higher AD and RD in WMH.
Zhang et al.[98] (2021)	Patients with lumbar puncture (n=39) and cSVD (n=330)	DTI-ALPS index	PVWMH and DWMH	Negative correlations between DTI-ALPS index and Fazekas grades of both PVWMH and DWMH.
Mayer et al.[70] (2022)	Population-based cohort study (n=900)	FW, FW-corrected FA (FA-t)	PVWMH and DWMH	Higher FW and lower FA-t in both PVWMH and DWMH.
Ferris et al.[71] (2022)	Normal (n=47) and stroke (n=33)	FA, MD MWF, GMT2	All WMH	Lower FA, and higher MD and GMT2 in WMH. Lower MWF in WMH among stroke patients, but not among older adults without stroke.
Haddad et al.[72] (2022)	Cerebrovascular disease (n=152)	FA, MD	PVWMH and DWMH	Lower FA and higher MD in both PVWMH and DWMH.
Zhang et al.[133] (2022)	cSVD (n=92)	CBF	All WMH	Lower CBF in WMH. Negative correlation between CBF and WMH volume.

Table 1. Continued

Study	Subjects	MRI features	Spatial classification	Main findings
Parent et al.[57] (2023)	Alzheimer's disease spectrum (n=118)	R1, R2*, T1w/T2w	All WMH	Lower R1, R2*, and T1w/T2w in WMH.
Lim et al.[126] (2025)	Normal and cognitive impairment (n=193)	K_{trans}, V_p	PVWMH and DWMH	Higher K_{trans} and lower V_p in PVWMH. No difference in K_{trans} and V_p between DWMH and NAWM. Negative correlations between K_{trans} or V_p and WMH volume in both PVWMH and DWMH.
Voorter et al.[84] (2025)	cSVD (n=76)	FW-corrected MD (MD-t), FW PS, V_p f	PVWMH and DWMH	Higher MD, FW, and PS, and lower f in both PVWMH and DWMH. Higher V_p in PVWMH but not in DWMH.
Wang et al.[92] (2025)	Patients with WMH (n=19)	D, D*, f	All WMH	Lower D and D*, and higher f in WMH.
Thammasart et al.[56] (2025)	Dementia spectrum (n=300)	CBF	JVWMH, PVWMH, and DWMH	Lower CBF in all WMHs.

MRI, magnetic resonance imaging; WMH, white matter hyperintensity; NAWM, normal-appearing white matter; TIA, transient ischemic attack; cSVD, cerebral small vessel disease; CBF, cerebral blood flow; MTT, mean transit time; FA, fractional anisotropy; MD, mean diffusivity; AD, axial diffusivity; RD, radial diffusivity; MTR, magnetization transfer ratio; NAA, N-acetylaspartate; Cr, creatine; Cho, choline; R1, longitudinal relaxation rate; D, parenchymal diffusion; D*, pseudo-diffusion; f, perfusion fraction; FDG-PET, 2-[^{18}F]fluoro-2-deoxy-D-glucose positron emission tomography; rSUV, regional standardized uptake value; V_{MY}, myelin partial volume; R2*, effective transverse relaxation rate; H_2O, tissue water content; f_{bound}, bound proton fraction; V_L, leakage volume; T_w, white matter-like signal fraction; T_g, gray matter-like signal fraction; T_c, cerebrospinal fluid-matter-like signal fraction; K_i, leakage rate; DTI-ALPS, diffusion tensor imaging analysis along the perivascular space; FW, free water; MWF, myelin water fraction; GMT2, geometric mean T2; T1w/T2w, T1-weighted and T2-weighted signal ratio; K_{trans}, volume transfer constant; V_p, plasma volume fraction; PS, permeability–surface area product; PVWMH, periventricular WMH; DWMH, deep subcortical WMH; JVWMH, juxtaventricular WMH.

selves convey additional clinically relevant information.[53]

Historically, WMHs were categorized into PVWMH and DWMH subtypes based on visual assessment of their spatial relationship to the lateral ventricles.[3,23-25,42,54] The principal criterion was continuity with the ventricular wall: PVWMH were defined by direct contact with the lateral ventricular wall, whereas DWMH were spatially separate. In practice, this rule proved fragile. With WMH progression, confluent PVWMH often merges with DWMH, obscuring boundaries. Inconsistent use of ancillary features (e.g., lesion shape), arbitrary distance thresholds, and divergent reassignment rules for large or irregular lesions further undermined reproducibility, likely contributing to cross-study heterogeneity in reported prevalence, risk factors, and clinical associations.[20,42] To enhance objectivity—even if modestly—contemporary schemes adopt explicit distance-based taxonomies measured from the ventricular surface. An extended framework[20,54-57] further links spatial location to putative mechanistic distinctions, thereby reducing inter-study variability. It delineates four territories: juxtaventricular WMH (JVWMH), contiguous with the ependyma within ~0–3 mm of the ventricle; PVWMH, occupying the periventricular "border-zone" at ~3–13 mm; DWMH, located at ≥~13 mm; and juxtacortical WMH (JCWMH), within ~4 mm of the corticomedullary junction. This distance-informed classification reduces ambiguity and provides a spatial framework that facilitates interpretation of lesion location in relation to biologically relevant patterns.

Microstructural alterations revealed by diffusion-based models of tissue water dynamics

Postmortem histopathology indicates that WMH lesions include axonal loss and demyelination[16,18,19,58]; these changes reduce fiber coherence and expand the extracellular space, thereby altering water diffusion and tissue water content (H_2O).[59]

Diffusion tensor imaging (DTI) quantifies directional water diffusion along white matter tracts by modeling diffusion anisotropy.[60,61] It is derived from DWI, which measures the mobility of water molecules constrained by tissue microstructure.[62,63] In intact tissue, axons and myelin restrict diffusion—particularly perpendicular to fibers—whereas in WMH, the loss of these microstructural barriers permits more isotropic diffusion of water molecules.[59]

Standard DTI metrics include fractional anisotropy (FA), reflecting directional coherence; mean diffusivity (MD), reflecting overall diffusivity; axial diffusivity (AD), diffusion along the principal axis; and radial diffusivity (RD), diffusion perpendicular to fibers (Figure 1B). These metrics have been histologically validated as markers of white matter microstructure, primarily capturing aspects of axonal organization rather than myelin den-

https://doi.org/10.5853/jos.2025.04168

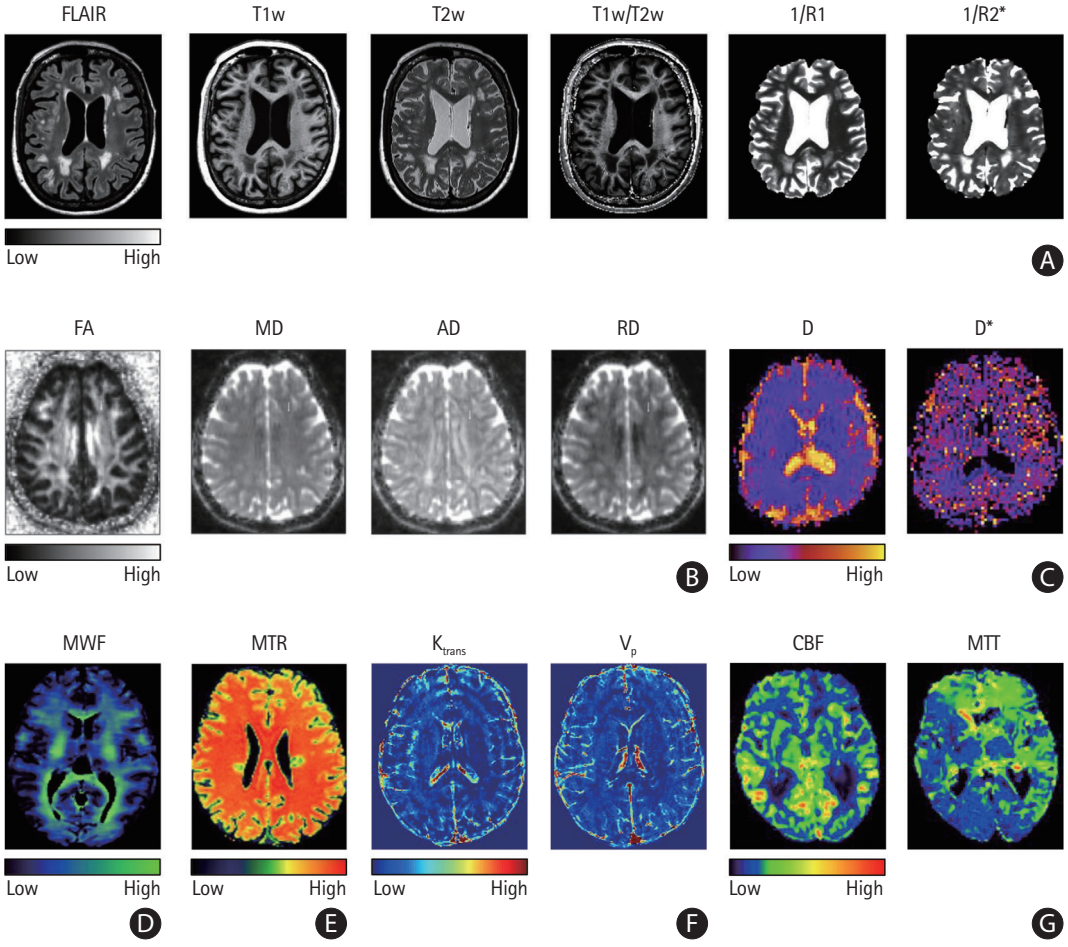

Figure 1. Representative multimodal magnetic resonance imaging (MRI) metrics for white matter research. (A) Structural MRI: fluid-attenuated inversion recovery (FLAIR), T1-weighted (T1w), T2-weighted (T2w), T1w/T2w ratio, longitudinal relaxation rate (R1), and effective transverse relaxation rate (R2*). Adapted from Parent et al. *Brain Commun* 2023;5:fcad279.[57] (B) Diffusion tensor imaging: fractional anisotropy (FA): mean diffusivity (MD), axial diffusivity (AD), and radial diffusivity (RD). Adapted from Gloor et al. *Eur Radiol* 2024;34:1680-1691.[215] (C) Intravoxel incoherent motion MRI: parenchymal diffusion (D) and pseudo-diffusion (D*). Adapted from Liao et al. *Front Hum Neurosci* 2021;15:617152.[225] (D) Myelin water imaging: myelin water fraction (MWF) map. Adapted from Dvorak et al. *Sci Adv* 2023;9:eadh9853.[226] (E) Magnetization transfer imaging: magnetization transfer ratio (MTR). Adapted from Meijboom et al. Wellcome *Open Res* 2022;7:94.[216] (F) Dynamic contrast-enhanced MRI: volume transfer constant (K_{trans}) and plasma volume fraction (V_p). Adapted from Ulas et al. *Front Neurol* 2019;9:1147.[227] (G) Dynamic susceptibility contrast MRI: cerebral blood flow (CBF) and mean transit time (MTT). Adapted from Kossen et al. *Front Neurol* 2023;13:1051397.[228] All adapted MRI panels have been modified and reproduced under the Creative Commons Attribution 4.0 International License (CC BY 4.0; https://creativecommons.org/licenses/by/4.0/).

sity.[64-66] Compared with NAWM, WMHs consistently shows lower FA[27,67-72] and higher MD[27,67-69,71,72] and RD,[67,73] consistent with reduced fiber coherence and extracellular space expansion.[16]

Notably, and contrary to expectation, AD is often higher in WMH than in NAWM.[67,69,73] Because AD reflects diffusion along the principal fiber axis, this elevation does not indicate preserved axons. Rather, it likely reflects tissue rarefaction—including vasogenic edema, myelin and cellular loss, and matrix disorganization—that reduces diffusion barriers, and elevates MD and RD and, sometimes, AD.[74,75] By contrast, AD decreases, when present, likely indicate advanced, chronic axonal disruption and collapse.[76,77]

Diffusion kurtosis imaging (DKI) extends DTI by capturing non-Gaussian diffusion arising from tissue complexity, with summary measures such as mean kurtosis (M_k), axial kurtosis (A_k), and radial kurtosis (R_k).[78,79] Recent postmortem studies confirmed histological correlations between DKI metrics and demyelination, both in humans[80] and in rodent models.[81-83]

More advanced models further estimate the free water (FW) fraction, which is typically elevated in and around WMH[70,84] and corresponds to the characteristic FA↓/MD↑/RD↑ profile, indicating extracellular expansion and edema. However, direct histological validation of FW fraction remains limited because fixation and postmortem shrinkage alter extracellular geometry and remove FW.[85]

Intravoxel incoherent motion (IVIM) imaging based on multi-b-value DWIs separates true parenchymal diffusion (D) from microvascular pseudo-diffusion (D*), yielding three parameters: D

coefficient, D* coefficient, and the perfusion fraction (f), the latter reflecting relative microvascular volume (Figure 1C).[86,87] This separation is possible because microvascular perfusion contributes predominantly to the diffusion signal at low b-values but diminishes at higher b-values, allowing model-based quantification of perfusion-related effects that would otherwise confound tissue water diffusion measurements. IVIM metrics have been validated in both phantom- and histology-based studies to effectively disentangle diffusion and perfusion components.[88,89]

IVIM-derived D—minimizing vascular contamination—is generally higher in WMH relative to NAWM,[87,90,91] providing information comparable to DTI-based metrics. A small pilot study (n=19), however, reported lower D values in WMH, possibly reflecting neovascularization, although the limited sample size precludes firm inference.[92] f is also typically higher in WMH than in NAWM,[87,90,92] likely reflecting compensatory microcirculatory vasodilation that maintains oxygen delivery following white matter ischemia.[90,93,94] However, a recent study has reported lower f in WMH,[84] underscoring methodological variability and the need for standardized analysis. Findings for D* remain inconsistent across studies,[87,90,92] likely due to differences in acquisition protocols, lesion topography, and NAWM definitions (e.g., inclusion or exclusion of perilesional tissue). A decrease in D* may be biologically plausible—consistent with reduced cerebral blood flow (CBF) from vascular rarefaction, arteriolar tortuosity, or venous collagen deposition[95]—yet a report of increased D* highlights the parameter's limited robustness (low signal-to-noise ratio) and model sensitivity, warranting cautious interpretation.[87]

Single-shell 3-tissue constrained spherical deconvolution, also derived from DWI, enables voxelwise characterization of WMHs by decomposing the diffusion signal into three tissue-like signal fractions—white matter-like (T_w), gray matter-like (T_g), and CSF-like (T_c)—further providing a compositional description of microstructural change.[96] These tissue-like compartments do not directly represent pathology but indicate the degree of similarity to healthy tissue profiles; an increased CSF-like fraction may reflect interstitial fluid expansion or rarefaction, whereas an increased T_g may indicate gliosis within white matter. Multi-tissue diffusion modeling further demonstrates a shift toward T_c and away from T_w within WMH, underscoring a compositional transition toward fluid-rich, structurally degraded tissue.[55,97]

Perivascular diffusion and glymphatic clearance dysfunction

Beyond microstructural and diffusional alterations, water mobility along perivascular spaces (PVS) provides additional insight into glymphatic clearance dysfunction, another key mechanism implicated in WMH pathology. The DTI analysis along the perivascular space (DTI-ALPS) index quantifies water diffusivity along these spaces, with lower values suggesting impaired glymphatic clearance associated with WMH.[98-100] This index is calculated in regions adjacent to the lateral ventricles, where medullary veins—and their accompanying PVS—run perpendicular to major projection and association fibers. This geometric arrangement allows estimation of water diffusivity that predominantly reflects perivascular flow with minimal contamination from surrounding white matter tracts. However, interpretation of the DTI-ALPS index as a direct measure of glymphatic function should be approached with caution, as it primarily quantifies water motion rather than directly capturing the complex dynamics of interstitial fluid clearance.[101] Therefore, complementary methods are required for a more comprehensive evaluation of the glymphatic system. For example, enlarged PVS[102,103]—CSF-filled cavities best visualized on T2/FLAIR MRI[104]—are frequently contiguous with or adjacent to WMH[105,106] and are considered structural correlates of impaired CSF clearance through the glymphatic pathway.[107-109] Their enlargement may signify impaired interstitial fluid drainage and reduced glymphatic clearance.

Altered myelin and macromolecular integrity

Whereas DWI provides general indices of water diffusion and H_2O, quantitative MRI (qMRI) techniques aim to quantify myelin and related macromolecules more specifically.[16,66,110] qMRI complements structural imaging with measures sensitive to specific tissue properties. qMRI extends conventional structural imaging by providing calibrated, biologically meaningful measurements sensitive to myelination, iron content, and cell membrane integrity in the living brain. A range of derived techniques—including relaxation rate mapping, myelin partial volume (V_{MY}) and H_2O mapping, T1w/T2w ratio, myelin water imaging (MWI), and magnetization transfer imaging (MTI)—are collectively referred to here as qMRI approaches for *in vivo* characterization of macromolecular integrity. The longitudinal relaxation rate R1 (1/T1) is higher in myelin-rich tissue, whereas the effective transverse relaxation rate R2* (1/T2*) is more influenced by iron content (Figure 1A).[111-116] Additional parameters include V_{MY}—a more direct estimate of myelin content—and H_2O, which indexes edema.[117] Together, R1, R2*, V_{MY}, and H_2O constitute a practical panel for probing tissue integrity. Across studies, WMHs compared with NAWM consistently show lower R1 (1/T1),[27,57,118] R2* (1/T2*),[57,118] and V_{MY},[119] along with higher H_2O,[118] a pattern indicative of demyelination and tissue rarefaction. The T1w/T2w ratio, derived from conventional T1 and T2-weighted MRIs, is a particularly accessible proxy for myelin content[120] and shows lower values in WMHs (vs. NAWM).[57]

MWI offers greater specificity[121-123] than other qMRIs or DTI

https://doi.org/10.5853/jos.2025.04168

methods by quantifying the myelin water fraction (MWF) (Figure 1D) and the geometric mean T2 (GMT2), the latter indexing interstitial fluid content.[71] MWF is reduced within WMHs among stroke cohorts but not consistently in older adults without stroke,[71] underscoring that demyelination cannot be inferred solely from DTI/qMRI, as other microstructural processes may predominate. In contrast, GMT2, indexing interstitial water, is elevated in WMHs,[71] aligning with higher H_2O and FW. The combination of marked GMT2 increases with only modest or absent MWF reductions supports the view that fluid-driven alterations, rather than frank myelin loss, often dominate WMH pathology.

MTI provides a more direct assessment of macromolecular content than DWI, by quantifying magnetization exchange between protons bound to macromolecules (e.g., myelin) and those in the FW pool.[36,66,124,125] Its principal metrics include the magnetization transfer ratio (MTR) (Figure 1E) and the bound proton fraction (f_{bound}). Both MTR—reflecting macromolecular integrity[27,67,118]—and f_{bound}—myelin-related pool[118]—are reduced in WMHs compared with NAWM. Taken together, these modalities converge on evidence of myelin/macromolecular compromise in WMHs, although their specificity for demyelination per se remains limited and should be interpreted with caution.

Vascular permeability and perfusion deficits

BBB disruption is a key mechanism linking vascular pathology to WMH, mediated by endothelial tight-junction loss and elevated perivascular hydrostatic pressure that promote interstitial edema.[84,91,126,127] Dynamic contrast-enhanced MRI assesses BBB integrity by tracking the passage of intravenously administered gadolinium-based contrast agents.[35,128,129] In healthy tissue, the agent remains intravascular, whereas BBB disruption permits extravasation into the interstitium, producing time-dependent T1 signal changes.

Pharmacokinetic modeling of these curves yields quantitative indices of permeability and vascularity. Key parameters include the volume transfer constant (K_{trans}) and the permeability–surface area product (PS). Both K_{trans} and PS reflect contrast leakage. PS more directly indexes endothelial permeability, whereas K_{trans} is also influenced by perfusion flow rate; the plasma volume fraction (V_p) reflects intravascular plasma volume within tissue (Figure 1F). Increased Ktrans or PS indicates endothelial tight-junction breakdown and BBB dysfunction, whereas elevated V_p suggests increased intravascular volume (e.g., vasodilation or angiogenesis) as compensation for reduced permeability or inflammatory hyperemia. Additional leakage metrics—the influx rate constant (K_i, leakage rate) and leakage volume (V_L, spatial extent of leakage)—further quantify BBB permeability. Across studies, K_{trans},[126] PS,[84] K_i,[91] and V_L[91] are consistently higher in WMH than in NAWM, indicating impaired barrier function. Notably, K_{trans} elevations are usually confined to PVWMH (vs. NAWM) and not consistently seen in DWMH, suggesting region-specific mechanisms.[126] By contrast, V_p findings are heterogeneous—higher in cSVD cohorts,[84] but lower values in cognitively normal/impaired older adults[126]—likely reflecting sensitivity of V_p to cSVD-related intravascular determinants (arteriolosclerosis, venous collagenosis, capillary remodeling/rarefaction, and vasomotor dysregulation) as well as methodological variability. An additional observation is the inverse relationship between K_{trans} or V_p and WMH volume.[126] Although counterintuitive given the association between global WMH burden and leakage,[126] water-permeability imaging likewise shows a negative correlation between the BBB water exchange rate within WMH and WMH volume (r=-0.51).[127] A plausible interpretation is that BBB leakage predominates early, whereas chronic lesions undergo tissue loss and reduced microvascular surface area, resulting in lower measured permeability and vascular volume. Analogous to multiple sclerosis, chronic WMHs may evolve toward atrophic,[130] low perfusion states with diminished vascular metrics.

Chronic hypoperfusion also contributes to WMH formation[56,69,118,131-133] by inducing rarefaction of myelin sheaths[134-136] and glial activation[134,137-139] via excitotoxicity, oxidative stress, BBB dysfunction, and secondary inflammation.[140,141] Cerebral perfusion can be assessed with dynamic susceptibility contrast (DSC) MRI—which tracks contrast agents to quantify hemodynamics—and arterial spin labeling (ASL), which magnetically labels arterial water to quantify its delivery to brain tissue.[37,142] The principal metric is CBF, expressed as mL of blood delivered per 100 g of brain tissue per minute (Figure 1G). DSC also provides cerebral blood volume (CBV) and mean transit time (MTT) (Figure 1G)—the average duration of microvascular transit. Independent evidence from DSC-MRI and ASL consistently show reduced CBF[56,69,118,131-133] and prolonged MTT[112] within WMHs relative to NAWM, providing *in vivo* support for chronic hypoperfusion[143] as a major contributor to WMH development.

Metabolic disturbances

WMHs show metabolite alterations consistent with microstructural injury and impaired cellular energy metabolism.[144-146] MR spectroscopy (MRS) provides a non-invasive *in vivo* "chemical biopsy" of brain tissue by quantifying metabolite concentrations.[38,147] The most widely used technique, proton (^{1}H) MRS, measures molecules such as N-acetylaspartate (NAA)—a marker of neuronal and axonal integrity[148,149]—choline (Cho), which reflects membrane turnover and increases with myelin breakdown or gliosis,[148,150] and creatine (Cr), an index of cellular energy metabolism.[148,151] These metabolites are well-validated for reliable

comparative quantification in both clinical and research contexts.[152,153] Within WMH, ^{1}H-MRS typically shows reduced NAA (or NAA/Cr)[144,145] and reduced Cr[144] relative to NAWM, indicating diminished neuronal/axonal integrity (NAA) and impaired energy metabolism (Cr), respectively. A biphasic Cho/Cr pattern has been observed in the anterior horn region[145]: lower values in mild–moderate WMH but higher values in severe WMH compared with controls, suggesting early Cho elevation (reflecting membrane turnover or glial proliferation) followed by decline as irreversible injury accumulates and reparative capacity fails.

Reduced glucose uptake in white matter has also been linked to neuroglial dysfunction associated with WMH. 2-[^{18}F]fluoro-2-deoxy-D-glucose positron emission tomography (FDG-PET) visualizes cerebral glucose metabolism,[154,155] which normally parallels regional synaptic activity and declines with synaptic dysfunction or neurodegeneration. In white matter, axonal conduction and myelin maintenance impose substantial energetic demands on the oligodendrocyte–axon unit[156,157]; accordingly, WMH-related disruption of neuroglial support is expected to lower FDG uptake.[68]

Summary

Multimodal MRI converges on a composite WMH pathobiology marked by tissue rarefaction and extracellular fluid expansion (FA↓, MD/RD↑, FW↑, T_c↑/T_w↓, GMT2↑, H_2O↑), variably accompanied by axonal injury (AD often ↑ with barrier loss, but ↓ in advanced collapse) and context-dependent demyelination (R1↓, T1w/T2w↓, MTR↓, V_{MY}↓; MWF↓ primarily in high-risk cohorts). Perivascular diffusion metrics and PVS enlargement indicate impaired glymphatic clearance (ALPS↓), suggesting failure of interstitial fluid drainage. Quantitative and magnetization-based measures converge on macromolecular compromise, while vascular signatures reveal BBB dysfunction (K_{trans}/PS/K_i/V_L↑), heterogeneous V_p behavior across cohorts, and chronic hypoperfusion (CBF↓, MTT↑; D* tending ↓, f often ↑ via compensatory vasodilation). Metabolic imaging demonstrates impaired neuronal/axonal integrity and energy metabolism (NAA↓, Cr↓, FDG-PET regional standardized uptake value [rSUV]↓) with stage-dependent choline shifts reflecting early gliosis followed by exhaustion of reparative capacity. Collectively, these modalities depict WMH as a multifactorial process integrating microstructural degradation, vascular and glymphatic failure, and metabolic insufficiency.

Multimodal MRI signatures of PVWMH versus DWMH

Spatial classification remains a practical framework for understanding WMH heterogeneity.[20] Along the ventricle-to-cortex axis, PVWMHs exhibit histopathological features of ependymal discontinuity, subependymal gliosis, loosening of the fiber matrix with myelin pallor, and tortuous venules.[19,21,158,159] Age-related loss of myelin basic protein and reduced small-vessel density in PV regions promote interstitial water accumulation.[17] Together with periventricular venous collagenosis[160,161] and BBB dysfunction,[22] these findings support a PVWMH pathobiology dominated by periventricular interstitial edema secondary to ependymal disruption, compounded by BBB leakage and venous wall remodeling. In contrast, DWMHs reflect arteriolosclerotic deep-perforator ischemia (chronic hypoperfusion), driving incomplete infarction with progressive myelin and axonal loss,[17,19,21,159,162-164] often accompanied by enlarged PVS. In short, location encodes mechanism: PVWMHs reflect a periventricular interstitial-edema/clearance phenotype with BBB leakage and venous remodeling, whereas DWMHs represent arteriolosclerotic deep-perforator ischemia and PVS-associated glymphatic phenotype. Here, we reevaluate this location-mechanism framework based on convergent multimodal MRI evidence, refining its mechanistic boundary conditions (Table 2).

Microstructural alterations revealed by diffusion-based models of tissue water dynamics

Relative to NAWM, both PVWMH and DWMH exhibit lower FA and higher MD, AD, and RD,[27,67-73] consistent with reduced fiber coherence and extracellular space expansion. Across multiple studies, FA is consistently lower in PVWMH than in DWMH.[54,72,165] One study that separated JVWMH (<3 mm from the ventricles) reported a gradient of FA reduction with ventricular proximity (DWMH > PVWMH > JVWMH).[54] T_c increases and T_w decreases closer to the ventricle (from DWMH to JVWMH),[55] indicating a shift toward a CSF-like composition, consistent with axon/myelin loss and interstitial fluid expansion. Another study[165] found particularly low FA in frontal PVWMH compared with occipital or parietal PVWMH, underscoring heterogeneity within PV regions. By contrast, MD, AD, and RD were highest in JVWMH, lowest in PVWMH, and intermediate in DWMH (JVWMH > DWMH > PVWMH), suggesting a potentially nonlinear ventricle-to-cortex gradient. A recent study[84] also reported higher FW (and MD) in PVWMH than in DWMH, supporting greater interstitial fluid accumulation and matrix rarefaction near the ventricles. Taken together, PVWMHs generally show more severe microstructural rarefaction and higher water content than DWMH, although PVWMHs located farther from the ventricles (>3 mm) may exhibit smaller changes—sometimes even less than those seen in DWMH.

IVIM-derived D is generally higher in WMH than in NAWM.[87,90,91] Notably, one study[90] reported greater D in PVWMH than in

https://doi.org/10.5853/jos.2025.04168

Table 2. Multimodal MRI signatures of PVWMH versus DWMH

Study	Subjects	MRI features	Spatial classification	Main findings
Spilt et al.[172] (2006)	Patients with WMH (n=56)	MTR	PVWMH and DWMH	Lower MTR in PVWMH vs. DWMH.
Promjunyakul et al.[176] (2015)	Normal (n=61)	CBF	PVWMH and DWMH	Lower CBF in PVWMH vs. DWMH.
Sun et al.[90] (2017)	Patients with WMH (n=32)	D	PVWMH and DWMH	Higher D in PVWMH compared to DWMH.
Promjunyakul et al.[69] (2018)	Cognitively normal (n=52)	CBF	PVWMH and DWMH	Lower CBF in PVWMH vs. DWMH.
Griffanti et al.[54] (2018)	Population-based cohort (n=525)	FA, MD, AD, RD	JVWMH, PVWMH, and DWMH	Lowest FA, and highest MD, AD, and RD in JVWMH compared to PVWMH and DWMH. Lower FA in PVWMH compared to DWMH. Lower MD, AD, and RD in PVWMH compared to DWMH.
Park et al.[119] (2019)	Cognitive complaints (n=99)	V_{MY}	PVWMH and DWMH	Lower V_{MY} in PVWMH compared to DWMH.
Iordanishvili et al.[118] (2019)	Non-demented normal (n=70)	R1, R2*, H_2O MTR, f_{bound}	PVWMH and DWMH	Lower R1, R2*, MTR, and f_{bound}, and higher H_2O in PVWMH compared to DWMH. Lower R1, R2*, and f_{bound}, and higher H_2O in Fazekas-3 DWMH compared to Fazekas-1 DWMH. Lower R2* in Fazekas-3 PVWMH compared to Fazekas-1 PVWMH.
Khan et al.[55] (2020)	Stroke (n=97)	T_w, T_g, T_c	JVWMH, PVWMH, and DWMH	Lowest T_w and highest T_c in JVWMH compared to PVWMH and DWMH. Lower T_w and higher T_c in PVWMH compared to DWMH.
Huang et al.[105] (2021)	Healthy older adults (n=136)	Enlarged dwPVS FW	DWMH	Connection of most DWMHs (89%) with enlarged dwPVS. Positive correlation between enlarged dwPVS volume and DWMH volume (mediated by FW).
Min et al.[165] (2021)	Normal and patients with WMH (n=91)	FA, MD, AD, RD	PVWMH (frontal, parietal, occipital) and DWMH (deep centrum ovale)	Lower FA and higher MD, AD, RD in frontal PVWMH compared to centrum ovale DWMH.
Barnes et al.[106] (2022)	Population-based cohort (n=29)	Enlarged dwPVS	DWMH	Adjacency to or enclosure by enlarged dwPVS for most DWMHs (~70%).
Haddad et al.[72] (2022)	Cerebrovascular disease (n=152)	FA, MD	PVWMH and DWMH	Lower FA and higher MD in PVWMH compared to DWMH.
Cai et al.[167] (2022)	Normal (n=152)	DTI-ALPS index CBF	PVWMH and DWMH	Negative correlation between DTI-ALPS index or CBF and DWMH volume.
Parent et al.[57] (2023)	Alzheimer's disease spectrum (n=118)	T1w/T2w, R1, R2*	PVWMH, DWMH, and JCWMH (superficial WM)	Negative correlation between T1w/T2w or R1 and WMH volume in DWMH and JCWMH. No significant correlation between T1w/T2w or R1 and WMH volume in PVWMH. Negative correlation between R2* and WMH volume in PVWMH and JCWMH. No significant correlation between R2* and WMH volume in DWMH.
Lim et al.[126] (2025)	Normal and cognitive impairment (n=193)	K_{trans}, V_p	PVWMH and DWMH	Higher K_{trans} and lower V_p in PVWMH compared to DWMH.
Voorter et al.[84] (2025)	cSVD (n=76)	MD, FW V_p	PVWMH and DWMH	Higher MD, FW, and V_p in PVWMH compared to DWMH.
Thammasart et al.[56] (2025)	Dementia spectrum (n=300)	CBF	JVWMH, PVWMH, and DWMH	Lowest CBF in JVWMH compared to PVWMH and DWMH. Lower CBF in PVWMH compared to DWMH.

MRI, magnetic resonance imaging; WMH, white matter hyperintensity; PVWMH, periventricular WMH; DWMH, deep subcortical WMH; cSVD, cerebral small vessel disease; MTR, magnetization transfer ratio; CBF, cerebral blood flow; D, parenchymal diffusion; FA, fractional anisotropy; MD, mean diffusivity; AD, axial diffusivity; RD, radial diffusivity; V_{MY}, myelin partial volume; R1, longitudinal relaxation rate; R2*, effective transverse relaxation rate; H_2O, tissue water content; f_{bound}, bound proton fraction; T_w, white matter-like signal fraction; T_g, gray matter-like signal fraction; T_c, cerebrospinal fluid-matter-like signal fraction; dwPVS, deep white matter perivascular space; DTI-ALPS, diffusion tensor image analysis along the perivascular space; T1w/T2w, T1-weighted and T2-weighted signal ratio; K_{trans}, volume transfer constant; V_p, plasma volume fraction; cSVD, cerebral small vessel disease; FW, free water; JVWMH, juxtaventricular WMH; JCWMH, juxtacortical WMH; DTI-ALPS, diffusion tensor imaging analysis along the perivascular space.

DWMH, consistent with higher interstitial water content attributed to increased BBB permeability and plasma leakage in PVWMH.[166]

Finally, the DTI-ALPS index—an estimate of diffusion along perivascular pathways reflecting glymphatic clearance—was independently associated with DWMH volume but not PVWMH volume,[167] consistent with histopathological evidence[21,159,162-164] of more prominent enlarged PVS in deep white matter than in periventricular regions. By contrast, PVWMH volume was related to ALPS only indirectly via deep medullary vein remodeling: impaired perivascular clearance (lower ALPS) may promote venous injury and remodeling on a background of frequent periventricular venous collagenosis,[160,161] thereby compromising drainage and fostering interstitial edema and lesion expansion. DWMHs are frequently (70%–90%) located adjacent to enlarged deep white matter PVS (dwPVS),[105,106] and their volume scales with enlarged dwPVS burden.[105] In contrast, PVWMHs show limited proximity to PVS (including enlarged basal ganglia PVS [bgPVS]), indicating that PVS-related pathology is more characteristic of DWMH than PVWMH.[105] Nonetheless, multiple cohorts report that enlarged bgPVS severity correlates with overall WMH burden,[168-171] an association that is not location-specific and may reflect a more global microvascular or clearance dysfunction. Notably, FW within DWMH mediated the relationship between enlarged dwPVS and DWMH volume,[105] further supporting a mechanistic link via impaired interstitial fluid drainage.

Altered myelin and macromolecular integrity

Across myelin-related qMRI metrics, both PVWMH and DWMH show lower R1 (1/T1), R2* (1/T2*), V_{MY}, and T1w/T2w, together with higher H_2O, compared with NAWM.[27,57,118,119] Notably, PVWMH exhibits larger deviations than DWMH—lower R1 and R2* and higher H_2O—suggesting more pronounced myelin/macromolecular alterations toward the ventricles along the ventricle-to-cortex gradient.[118] Consistent with this, V_{MY} is lower in PVWMHs than in DWMHs,[119] supporting greater myelin/macromolecular compromise in periventricular regions. MTI-based indices show a similar pattern, with both MTR[118,172] (macromolecular integrity) and f_{bound}[118] (myelin-related pool) reduced in PVWMHs relative to DWMHs. However, direct MWI comparisons between PVWMHs and DWMHs remain scarce; accordingly, these qMRI and MTI differences should not be over-interpreted as specific evidence of demyelination.

Notably, declines in myelin/macromolecular indices (lower R1 or T1w/T2w) predict cross-sectional WMH volume (or Fazekas grade) within DWMH or JCWMH, but not within PVWMH.[57,118] By contrast, PVWMH volume (or Fazekas grade) shows a stronger association with lower R2*[57,118]—a metric influenced by paramagnetic iron concentrated in oligodendrocytes.[173,174] This dissociation suggests that demyelination and macromolecular degradation may be more central to DWMH/JCWMH progression, whereas PVWMH progression may be more tightly linked to iron-related oligodendrocyte vulnerability. Accordingly, lower qMRI values in PVWMH relative to DWMH should not be taken as evidence of greater myelin/macromolecular damage per se, but may instead reflect ventricle-adjacent CSF or iron effects and local vascular/ependymal pathology.

Vascular permeability and perfusion deficits

Across studies, K_{trans}, PS, K_i, and V_L are consistently elevated in WMH compared with NAWM, indicating increased BBB leakage.[84,91,126] K_{trans} is also higher in PVWMH than in DWMH, suggesting a more prominent contribution of BBB dysfunction to PVWMH pathobiology.[126] By contrast, V_p shows divergent results across cohorts—higher[84] in PVWMH among patients with cSVD but lower[126] in PVWMH among cognitively normal and impaired older adults—supporting the interpretation that V_p is sensitive to intravascular determinants (such as microvascular volume, arteriolosclerosis, venous remodeling) beyond BBB leakage, potentially accentuated near the ventricular CSF interface.[35,175]

Multiple studies report lower regional CBF in PVWMH than in DWMH,[56,69,176] with the lowest values in JVWMH.[56] However, these absolute CBF differences across JVWMH, PVWMH, and DWMH should be interpreted with caution. MRI-derived CBF is vulnerable to biases near the ventricles—prolonged arterial transit time and CSF partial-volume effects—that can artifactually depress periventricular estimates independent of true hypoperfusion.[133,177] Additionally, partial-volume contamination from gray matter—given the large gray matter–white matter perfusion contrast—can bias white matter CBF estimates, particularly in deep WMHs where voxels border deep gray nuclei (e.g., thalamus, basal ganglia), leading to artificially elevated WM perfusion values.[178,179] Consistent with this, one study reported a distance-to-ventricle effect, with progressively lower CBF in both WMH and perilesional NAWM closer to the ventricles.[56] Even so, lower CBF is also linked to perilesional NAWM abnormalities (penumbra),[78,176,180,181] new WMH,[56,69] and WMH lesion growth[69] in both PVWMH and DWMH, challenging the notion that chronic hypoperfusion is primarily a DWMH pathology. Plausible explanations include (1) sampling and interpretive limitations of prior histopathology and (2) tight coupling of CBF reductions to periventricular processes (interstitial fluid accumulation, BBB leakage), producing confounding. Future work should combine histopathologically anchored designs with confounder-controlled MRI perfusion methods—such as multi-post-labeling delay (arterial transit time-corrected) ASL—and integrate BBB and wa-

https://doi.org/10.5853/jos.2025.04168

ter-content indices to isolate hypoperfusion-specific effects.

Summary

Across modalities, PVWMH and DWMH share a core signature of microstructural injury (FA↓, MD/RD↑) but the primary type of damage differs. PVWMHs show greater extracellular fluid shifts (FW↑; diffusion composition T_c↑/T_w↓), more BBB leakage (K_{trans}↑), and larger deviations in myelin/macromolecular indices (R1/R2*/V_{MY}/MTR↓). This pattern is consistent with a periventricular interstitial-edema phenotype with BBB leakage and venous remodeling. By contrast, DWMHs are closely associated with PVS enlargement and lower ALPS, indicating impaired glymphatic drainage, while deep-perforator ischemia also contributes. Together, multimodal MRI indicates that PVWMHs are dominated by edema/clearance failure and BBB dysfunction, whereas DWMHs represent a PVS-associated glymphatic phenotype with a contributory role of deep perforator ischemia.

Multimodal MRI signatures in perilesional NAWM

Across studies sampling concentric layers around WMHs, multiple modalities demonstrate that NAWM within ~10 mm of a lesion exhibits systematic deviations relative to more distant NAWM (Table 3). These abnormalities diminish with increasing distance, supporting a continuum model in which perilesional NAWM contains subclinical injury that gradually normalizes. The operational "penumbra" width varies by modality—typically ~2–6 mm for microstructural and water content markers and up to ~8–14 mm for perfusion and BBB-related measures. Emerging evidence also suggests regional differences: periventricular lesions often display broader perfusion and leakage halos than deep lesions, consistent with location-dependent pathophysiology.

Microstructural alterations revealed by diffusion-based models of tissue water dynamics

Perilesional NAWM shows a distance-dependent, inverted-U-shaped FA profile: FA rises from distant NAWM toward ~4 mm from the WMH margin, then declines from ~4 mm to the lesion edge.[27,28,70,71,78,180,181] Accordingly, perilesional NAWM may show either higher[27,28,70,78,181] or lower[26,67,71,180] FA than distant NAWM depending on the sampling radius and study design. When PVWMHs and DWMHs are analyzed separately, the inverted-U profile is more pronounced around PVWMH,[78,180,181] likely reflecting location effects—PVWMHs abut highly coherent commissural and association fibers (e.g., corpus callosum) where diffusion anisotropy is intrinsically high.[27] Other diffusion parameters (MD/AD/RD) are generally elevated in perilesional NAWM compared with distant NAWM.[27,28,67,71,78,84,180,181] Penumbra size defined by MD (or M_K)[28,71,78,84,180,181] ranges 2–12 mm, with most estimates 4–7 mm; in the single study[78] quantifying AD (or A_K) and RD (or R_K) gradients, the AD-defined penumbra extended 5–14 mm and the RD-defined penumbra 6–11 mm. Across studies,[78,84,180,181] PVWMH and DWMH differ in penumbra extent, although the direction varies across datasets and metrics, reflecting heterogeneity in lesion topography and penumbra definitions. Larger samples, finer spatial classification, and harmonized criteria are needed to resolve these discrepancies. Consistent with diffusion metrics, FW is higher in perilesional NAWM compared to distant NAWM,[70,84] with penumbra size estimated at ~4–8 mm and similar between PVWMHs and DWMHs. A decreasing IVIM f toward the WMH edge, together with rising FW, supports a pattern of predominantly extravascular fluid accumulation rather than increased intravascular volume.[84] In one longitudinal study,[91] D increased over 2 years with a distance-dependent gradient—greater in perilesional NAWM than in distant NAWM—indicating faster microstructural damage in the perilesional zone, consistent with prior DTI findings.

Altered myelin and macromolecular integrity

In NAWM immediately adjacent to PVWMH (<2 mm), R1 (1/T1)[27,28] is higher but MTR[27,67] is lower than in distant NAWM, with both measures lowest within WMH—yielding an inverted-U profile similar to that observed for DTI-FA. Although direct PVWMH-DWMH comparisons of R1/MTR are limited, this pattern likely reflects a location effect, given the predominance of PV-adjacent lesions. One study[67] also reported greater MTR reduction in frontal NAWM adjacent to PVWMH compared with parietal–occipital NAWM, highlighting spatial heterogeneity within periventricular regions and reinforcing the role of location effects. Notably, MWI demonstrated higher GMT2 (interstitial water) in perilesional NAWM (<6 mm) than in distant NAWM, whereas MWF did not differ across 2–10-mm shells, suggesting that fluid-driven changes, rather than overt demyelination, may predominate in the early penumbra.[71]

Vascular permeability and perfusion deficits

Perilesional NAWM exhibits a distance-dependent rise in BBB leakage, increasing from distant NAWM toward the WMH margin and peaking within the lesion.[28] In one study, PS and V_p showed little variation across perilesional NAWM,[84] whereas other studies reported progressive increases in K_i[91] and V_L[91,182] with proximity to the lesion, reaching their highest values within WMH. Notably, baseline BBB leakage (K_i and V_L) correlated with 2-year increases in D in the perilesional zone,[91] supporting

Table 3. Multimodal MRI signatures in perilesional NAWM (WMH penumbra)

Study	Subjects	MRI features	Spatial classification	Perilesional WM definition	Main findings
Bastin et al.[67] (2009)	Non-demented normal (n=42)	FA, RD, MTR	PVWMH (DWMH not examined)	A region of high PVWMH prevalence, though not explicitly defined	Lower FA and MTR, and higher RD in NAWM of subjects with PVWMH compared to those without.
Maillard et al.[26] (2011)	Alzheimer's disease spectrum (n=208)	FA	All WMH	Defined by NWI score, which is elevated in NAWM near WMH	Negative correlation between FA and NWI score.
Maniega et al.[27] (2015)	Population-based cohort (n=676)	R1 FA, MD MTR	All WMH	Concentric 2-mm layers from WMH border (up to 10 mm)	Increase in MD from outer NAWM toward WMH edge, with a reduction in MTR. Inverted-U profile for R1: increase from outer NAWM to ~4 mm from WMH border, then decrease toward WMH. Inverted-U profile for FA: increase from outer NAWM to ~4 mm from WMH border, then decrease toward WMH.
Promjunyakul et al.[176] (2015)	Normal (n=61)	CBF	PVWMH and DWMH	Concentric 1-mm layers from WMH border (up to 15 mm)	Lower CBF in perilesional NAWM compared to total brain NAWM; ~12 mm for PVWMH and ~11 mm for DWMH.
Promjunyakul et al.[180] (2016)	Normal (n=82)	CBF FA, MD	PVWMH and DWMH	Concentric 1-mm layers from WMH border (up to 15 mm)	Lower CBF in perilesional NAWM vs. total brain NAWM; penumbra of ~13 mm for PVWMH and ~14 mm for DWMH. Lower FA and higher MD in perilesional NAWM vs. next layer NAWMs; max 5 mm for PVWMH and max 9 mm for DWMH.
Wardlaw et al.[28] (2017)	cSVD or mild stroke (n=201)	BBB leakage FA, MD R1	All WMH	Concentric 2-mm layers from WMH border (up to 10 mm)	Linear increase in BBB leakage closer to WMH edge. Decreased FA with increasing proximity to WMH. Increased MD from the 4-mm contour proximate to WMH edge. Inverted-U profile for R1: increase from outer NAWM to ~4 mm from WMH border, then decrease toward WMH.
Wu et al.[181] (2019)	svMCI (n=73)	CBF FA, MD	PVWMH and DWMH	Concentric 1-mm layers from WMH border (up to 15 mm)	Lower CBF in perilesional NAWM vs. total brain NAWM; penumbra of ~10 mm for PVWMH and ~7 mm for DWMH. Lower FA and higher MD in perilesional NAWM vs. next layer NAWMs; max 6 mm for PVWMH and max 4 mm for DWMH.
Wong et al.[182] (2019)	cSVD (n=27)	CBF V_L	All WMH	Concentric 2-mm layers from WMH border (up to 10 mm)	Decreasing CBF and increasing V_L with closer to the WMH edge.
Kerkhofs et al.[91] (2021)	cSVD (n=43)	K_i, V_L ΔD	All WMH	Concentric 2-mm layers from WMH border (up to 12 mm)	Increasing baseline K_i and V_L closer to the WMH edge. Decreasing longitudinal D increase with greater distance from WMH.
Ferris et al.[71] (2022)	Normal (n=47) and stroke (n=33)	FA, MD GMT2	All WMH	Concentric 2-mm layers from WMH border (up to 10 mm)	Decreasing FA closer to WMH edge; ~4 mm penumbra. Increasing MD and GMT2 from outer NAWM toward WMH edge; ~4 mm penumbra for MD and ~6 mm penumbra for GMT2.
Mayer et al.[70] (2022)	Population-based cohort study (n=900)	FW, FW-corrected FA (FA-t)	PVWMH and DWMH	Concentric 2-mm layers from WMH border (up to 16 mm)	Higher FW in ~8 mm perilesional NAWM compared to the next layer NAWMs (in both PVWMH and DWMH). Inverted-U profile for FA-t: slight increase until 4 mm from WMH edge, followed by a decrease.

Table 3. Continued

Study	Subjects	MRI features	Spatial classification	Perilesional WM definition	Main findings
Wang et al.[78] (2023)	cSVD (n=42)	CBF FA, AD, MD, RD, M_k, A_k, R_k	PVWMH and DWMH	Concentric 1-mm layers from WMH border (up to 15 mm)	Lower CBF in perilesional NAWM vs. whole-brain NAWM; penumbra of ~14 mm for PVWMH and ~13 mm for DWMH. Lower FA, M_k, A_k, and R_k, and higher AD, MD, and RD in perilesional NAWM vs. next layer NAWMs; max 14 mm for PVWMH and max 8 mm for DWMH.
Vooter et al.[84] (2025)	cSVD (N=76)	FW-corrected MD (MD-t), FW, f	PVWMH and DWMH	Concentric 2-mm layers from WMH border (up to 10 mm)	Increasing MD-t and FW, and decreasing f closer to the WMH edge in both PVWMH and DWMH. PVWMH penumbra size: MD-t (2.4 mm), FW (4.0 mm), f (3.2 mm). DWMH penumbra size: MD-t (2.7 mm), FW (4.6 mm), f (1.6 mm).
Thammasart et al.[56] (2025)	Dementia spectrum (N=300)	CBF	All WMH	Regions at 4 and 8 mm from WMH border	Decreasing baseline CBF closer to the WMH edge.

MRI, magnetic resonance imaging; NAWM, normal-appearing white matter; WMH, white matter hyperintensity; cSVD, cerebral small vessel disease; svMCI, subcortical vascular mild cognitive impairment; FA, fractional anisotropy; RD, radial diffusivity; MTR, magnetization transfer ratio; R1, longitudinal relaxation rate; MD, mean diffusivity; CBF, cerebral blood flow; BBB, blood–brain barrier; V_L, leakage volume; K_i, leakage rate; D, parenchymal diffusion; GMT2, geometric mean T2; FW, free water; AD, axial diffusivity; M_k, mean kurtosis; A_k, axial kurtosis; R_k, radial kurtosis; f, perfusion fraction; PVWMH, periventricular WMH; DWMH, deep subcortical WMH; NWI, neighborhood white matter injury.

the hypothesis that early BBB impairment contributes to subsequent white matter degeneration. The minimal gradients in PS and V_p, contrasted with significant K_i and V_L changes, are most plausibly explained by differential model sensitivities for BBB permeability estimation (Tofts vs. Patlak).[183] Further studies are needed to clarify how these metrics diverge in practice and which offers superior prognostic value for BBB dysfunction in WMH.

Multiple studies consistently reported lower regional CBF in perilesional NAWM than in distant NAWM, with the lowest CBF values observed within WMH.[56,78,176,180-182] The CBF-defined penumbra typically spans 7–14 mm and appears broadly similar for PVWMH and DWMH. In studies that derived DTI-defined (structural) penumbras in parallel,[78,180,181] the CBF-defined penumbra was generally broader; in one study,[78] however, this divergence was observed only for DWMH, a finding that warrants more precise replication.

Summary

Across modalities, perilesional NAWM functions as an intermediate injury zone with distance-dependent gradients that normalize with increasing separation from the WMH core. Microstructural rarefaction and extracellular fluid expansion intensify near lesions (MD/AD/RD↑, FW↑), while FA (and R1) follows an inverted-U profile peaking around 4 mm from the margin. In PV-adjacent NAWM, myelin/macromolecular indices (e.g., MTR) mirror this pattern, whereas elevated GMT2 without clear MWF reduction indicates that fluid-driven alterations, rather than overt demyelination, dominate early injury. Vascularly, BBB leakage (K_i, V_L) increases toward the lesion edge, and baseline leakage predicts subsequent D increases (ΔD), linking early barrier dysfunction to progressive microstructural decline. Perfusion deficits (CBF↓) extend beyond the structural (diffusion) penumbra (~7–14 mm vs. ~2–6 mm), suggesting that hemodynamic compromise outpaces tissue degeneration. Collectively, these findings support the view that perilesional NAWM forms a dynamic continuum of injury—a pathophysiologically informative zone at risk that underscores the importance of harmonized definitions, spatially resolved analyses, and integrative multimodal metrics to improve prognostic assessment.

Multimodal MRI signatures of WMH progression

Follow-up studies commonly stratify white matter into persistent NAWM, constant WMH, and new WMH (voxels classified as NAWM at baseline that convert to WMH).[29,31,56,69] This framework connects cross-sectional signatures in NAWM, perilesional NAWM, and baseline WMH to longitudinal change, thereby

extending mechanistic insight into the heterogeneity of WMH pathobiology (Table 4).

Microstructural alterations revealed by diffusion-based models of tissue water dynamics

Multiple studies consistently reported lower baseline FA[29,31,68,69,184,185] and higher baseline MD[31,68,69,185] in regions that subsequently develop into new WMHs compared with persistent NAWM. One study[69] observed higher baseline AD and RD, together with lower FA and higher MD, in both PVWMH and DWMH. Notably, baseline RD was positively associated with subsequent WMH growth across both lesion types.

Extending cross-sectional observations of the spatial proximity between DWMHs and enlarged dwPVS,[105,106] a longitudinal study found that ~70% of new DWMHs emerged around enlarged dwPVS at follow-up.[106] This pattern supports the interpretation that a major component of DWMH pathobiology reflects impaired interstitial fluid drainage along perivascular pathways.

Vascular permeability and perfusion deficits

Baseline CBF is lower in regions that develop into new WMHs than in persistent NAWM.[69,132] One study found this reduction confined to JVWMH and PVWMH, but not DWMH,[56] while another[69] reported that baseline CBF predicted PVWMH growth but not DWMH growth—consistent with a location effect.

Blood oxygenation level–dependent (BOLD) functional MRI provides an indirect measure of cerebral hemodynamics by detecting T2*-weighted signal changes driven by deoxyhemoglobin.[186,187] A central application is the assessment of cerebrovascular reactivity (CVR)—the BOLD response to a standardized vasoactive stimulus.[188-190] CVR can be measured from the BOLD changes by simpler breath-hold tasks[188,189] or using controlled gas paradigms that elevate end-tidal CO_2 while maintaining end-tidal O_2,[190] thereby inducing hypercapnia. As a vascular reserve biomarker, CVR—including its steady-state component (ssCVR), representing the magnitude of the vasodilatory response, and its dynamic component (tau), reflecting the speed of vascular adjustment—complements static perfusion measures by probing the capacity of the microvasculature to dilate.[191] These BOLD-based metrics distinguished future WMHs from persistent NAWM,[185,191] suggesting that impaired vasodilatory reserve, beyond low CBF, contributes to WMH progression.

Metabolic disturbances

One MRS study demonstrated longitudinal reduction in NAA and Cr—but not glutamate/glutamine, Cho, or myo-inositol—within WMHs, suggesting that neuronal/axonal integrity (NAA) and energy metabolism (Cr) are compromised in persistent lesions and may contribute to progression risk.[146] Complementing MRS, FDG-PET demonstrates lower baseline rSUV in new WMHs than in persistent NAWM,[68] indicating that metabolic impairment accompanies structural WM injury.

Summary

Across longitudinal studies, new WMHs show a convergent baseline signature of microstructural compromise (FA↓, MD/AD/RD↑) most pronounced in regions that subsequently enlarge—linking pre-existing tissue rarefaction to lesion formation. Baseline RD further predicts future growth, supporting its utility as a microstructural risk marker. Hemodynamically, new lesions originate from regions with reduced baseline CBF, while impaired vasodilatory reserve on BOLD-CVR (including ssCVR and tau) prospectively distinguishes tissue destined to convert from tissue that remains NAWM, indicating that vascular reactivity failure, beyond low flow alone, contributes to progression. Topographically, new DWMHs cluster around enlarged dwPVS, consistent with impaired interstitial fluid drainage as a location-specific mechanism. Metabolically, longitudinal reductions in NAA and Cr within persistent lesions indicate ongoing neuronal/axonal injury and energy dysfunction, while lower baseline FDG-PET rSUV in new WMHs supports metabolic disturbance as an additional driver of progression. Collectively, these observations underscore that WMH progression is a complex, multicomponent process shaped by interactions among microstructural vulnerability, vascular dysregulation, impaired perivascular drainage, and metabolic stress.

Mechanistic insights into heterogeneity in WMH pathobiology

The multimodal MRI evidence synthesized in this review converges on mechanistic frameworks that account for WMH heterogeneity across multiple dimensions. By integrating structural, vascular, and metabolic signatures, these frameworks delineate pathobiological subtypes that move beyond conventional lesion volume metrics.

Spatial heterogeneity: location-encoded mechanisms

The ventricle-to-cortex gradient emerges as a fundamental organizing principle for WMH pathobiology. Evidence indicates that PVWMHs and DWMHs represent mechanistically distinct entities rather than variants of a single process.

PVWMHs exhibit a characteristic profile of periventricular interstitial edema, marked by prominent BBB dysfunction (ele-

https://doi.org/10.5853/jos.2025.04168

Table 4. Multimodal MRI signatures of WMH progression (longitudinal follow-up studies)

Study	Subjects	Follow-up period	MRI features	Spatial classification	Main findings
Maillard et al.[29] (2013)	Alzheimer's disease spectrum (n=119)	3.7 (±1.8) years	FA	All WMH	Significant association of lower baseline FA with an increased risk for new WMH.
De Groot et al.[31] (2013)	General population (n=689)	3.5 years	FA, MD	All WMH	Lower baseline FA and higher baseline MD in new WMH compared to persistent NAWM.
Maillard et al.[184] (2014)	Cognitively normal (n=115)	2 years	FA	All WMH	Lower baseline FA in new (growing and incident) WMH compared to persistent NAWM.
Erdélyi-Bótor et al.[146] (2015)	Migraine (n=17)	3 years	NAA, Cr	All WMH	Longitudinal decrease in NAA and Cr within pre-existing WMH.
Bernbaum et al.[132] (2015)	Minor stroke/TIA (n=40)	18 months	CBF	All WMH	Lower baseline CBF in new WMH compared to persistent NAWM.
Sam et al.[185] (2016)	Patients with moderate to severe WMH (n=45)	1 year	CVR FA, MD	All WMH	Lower baseline CVR and FA, and higher baseline MD in new WMH compared to persistent NAWM.
Sam et al.[191] (2016)	Patients with moderate to severe WMH (n=45)	1 year	ssCVR, tau	All WMH	Lower baseline ssCVR and higher baseline tau in new WMH compared to persistent NAWM.
Promjunyakul et al.[69] (2018)	Cognitively normal (n=52)	17 months (ranging 7–54 months)	CBF FA, MD, AD, RD	PVWMH and DWMH	Lower baseline CBF and FA, and higher baseline MD, AD, and RD in new WMH vs. persistent NAWM (in both PVWMH and DWMH). Negative correlation of baseline CBF and positive correlation of baseline RD within NAWM with subsequent PVWMH growth. Positive correlation of baseline RD within NAWM with subsequent DWMH growth.
Jiaerken et al.[68] (2019)	Alzheimer's disease spectrum (n=40)	2 years	FA, MD FDG-PET rSUV	All WMH	Lower baseline FA and FDG-PET rSUV, and higher baseline MD, in new WMH compared to persistent NAWM.
Barnes et al.[106] (2022)	Population-based cohort (n=29)	3 years	Enlarged dwPVS	DWMH	Occurrence of most new DWMHs (~70%) around enlarged dwPVS.
Thammasart et al.[56] (2025)	Dementia spectrum (n=300)	2 years	CBF	JVWMH, PVWMH, and DWMH	Lower baseline CBF in new (growing) WMH compared to persistent NAWM near JVWMH and PVWMH; no difference for DWMH.

MRI, magnetic resonance imaging; WMH, white matter hyperintensity; TIA, transient ischemic attack; FA, fractional anisotropy; MD, mean diffusivity; NAA, N-acetylaspartate; Cr, creatine; CBF, cerebral blood flow; CVR, cerebrovascular reactivity; ssCVR, steady-state components of CVR; tau, dynamic components of CVR; AD, axial diffusivity; RD, radial diffusivity; FDG-PET, 2-[^{18}F]fluoro-2-deoxy-D glucose positron emission tomography; rSUV, regional standardized uptake value; dwPVS, deep white matter perivascular space; PVWMH, periventricular WMH; DWMH, deep subcortical WMH; JVWMH, juxtaventricular WMH; NAWM, normal-appearing white matter.

vated K_{trans}, PS, K_i, and V_L),[84,91,126] extensive extracellular fluid accumulation (increased FW and T_c).[55,84] This pattern aligns with histopathological evidence of ependymal disruption, subependymal gliosis, and periventricular venous collagenosis.[17,19,21,22,158-161] Moreover, the association between PVWMH progression and R2* reductions[57,118]—reflecting iron-related oligodendrocyte vulnerability—further distinguishes periventricular pathobiology from deep white matter changes.

In contrast, the DWMH phenotype is more robustly characterized by glymphatic dysfunction. A direct association between the DTI-ALPS index and DWMH volume,[167] together with the frequent colocalization of DWMHs with enlarged dwPVS,[105,106] implicates clearance failure as a central mechanism. FW further mediates the relationship between dwPVS burden and DWMH volume,[105] supporting a pathway in which impaired interstitial—perivascular drainage promotes extracellular fluid accumulation and lesion growth. Myelin and macromolecular integrity indices (R1 and T1w/T2w) also predict DWMH and JCWMH progression but not PVWMH volume,[57,118] suggesting that demyelination and macromolecular degradation are more prominent contributors to deep-lesion expansion.

Finally, the observation that MRI-derived CBF reductions are not specific to DWMH challenges the prevailing view of selective deep-perforator hypoperfusion and calls for re-examining vascular mechanisms across the ventricle-to-cortex continuum.[56,69,78,176,180,181] However, despite the limited specificity of CBF measurements alone, epidemiological and clinical studies have shown that DWMH correlate more strongly with cardiovascular mortality,[192] recurrent stroke (with larger risk ratios than PVWMH),[193,194] and vascular dementia,[195,196] whereas PVWMH exhibit closer associations with noncardiovascular mortality[192] and Alzheimer's disease.[195,196] These divergent patterns suggest that vascular pathology beyond BBB leakage—particularly ischemia-related demyelination and impaired clearance—may be more tightly linked to DWMH. Similarly, our recent work[15] in a consecutive stroke cohort (in which PVWMH predominated)[6] found that total WMH burden was more closely related to nonvascular mortality and hemorrhagic stroke recurrence. Thus, although ischemia is not exclusive to DWMH, these lesions may display greater susceptibility under comparable ischemic stress, a plausible hypothesis that merits prospective validation.

Temporal heterogeneity: longitudinal evolution of tissue injury

Longitudinal MRI signatures delineate a temporal cascade of pathobiological events driving WMH formation and progression. Pre-lesional tissue destined to evolve into WMH exhibits a characteristic baseline profile: microstructural compromise (lower FA and higher MD, AD, and RD),[27,28,67,70,71,78,84,180,181] reduced perfusion (lower CBF),[56,78,176,180-182] and impaired vascular reserve (abnormal CVR, ssCVR, and tau).[185,191] Notably, baseline RD predicts subsequent WMH growth,[69] establishing it as a mechanistic biomarker that links early myelin/axonal injury to later lesion expansion.

The perilesional penumbra constitutes a critical transition zone where pathobiological processes evolve. The observation that the hemodynamic penumbra (7–14 mm) is broader than the structural penumbra (2–6 mm)[78,180,181] suggests that perfusion deficits precede overt tissue damage. The correlation between baseline BBB leakage (K_i, V_L) and subsequent increase in D in perilesional NAWM[91] provides direct evidence for a vascular-driven progression toward structural injury. However, future studies investigating the structural penumbra should incorporate myelin-sensitive markers (e.g., R1, MWF, MTI) alongside conventional water diffusion metrics (e.g., FA, AD, MD, RD). While diffusion metrics are sensitive to microstructural disruption, they lack specificity and can be altered by ischemia-related changes in intravascular and plasma volumes even in the absence of substantial demyelination.[28,69,78,84,180,181] Within this framework, the inverted-U profile of FA and myelin indices (R1 and MTR) in perilesional NAWM likely reflects competing processes[27,28,70]: compensatory tissue reorganization at intermediate distances from the lesion and progressive degeneration near the lesion edge.

From imaging profiles to clinical practice

The multimodal MRI signatures synthesized in this review provide a translational bridge from pathobiological insights to clinical application. While total WMH burden is a well-established risk marker, fine-grained imaging profiles may enable more precise patient stratification, mechanism-specific therapeutic targeting, and longitudinal monitoring—moving beyond one-size-fits-all management strategies.

Risk stratification and therapeutic targeting based on spatial heterogeneity

Identifying a patient's predominant spatial phenotype has clinical relevance, as it reflects distinct underlying mechanisms that may demand different monitoring priorities and interventions.

PVWMH-predominant profile

The periventricular phenotype is characterized by BBB dysfunction (elevated K_{trans}, PS, K_i, and V_L),[84,91,126] and interstitial fluid accumulation (increased FW and T_c),[55,84] consistent with histopathologic evidence of ependymal disruption and venous remodeling.[17,19,21,22,158-161] Management can reasonably prioritize

https://doi.org/10.5853/jos.2025.04168

BBB stabilization (e.g., strict blood-pressure control)[197-199] and mitigation of periventricular interstitial edema. As a mechanism-aligned example, low-dose acetazolamide has been shown to reduce periventricular hyperintensity in idiopathic normal pressure hydrocephalus[200]; whether this extends to non-hydrocephalus WMH, including post-stroke populations, remains uncertain and warrants prospective confirmation. Surveillance can include R2*—a marker of oligodendrocyte vulnerability[173,174]—as a surrogate of PVWMH progression.[57,118] Agents with putative oligodendrocyte-protective effects, such as methylprednisolone[201] or minocycline,[202] are mechanistically plausible for PVWMH, though WMH/cSVD-specific clinical evidence is limited, and their use still remains investigational pending dedicated trials. This mechanism-anchored approach may also help lower the increased dementia risk—particularly Alzheimer's disease—associated with greater PVWMH burden.[195,196]

DWMH-predominant patterns

DWMH phenotypes are more tightly linked to glymphatic and clearance dysfunction (lower DTI-ALPS[167] and colocalization with dilated deep PVS[105,106]), with progression more consistently tracked by myelin/macromolecular indices (R1 and T1w/T2w).[57,118] Therapeutic strategies should thus emphasize enhancing perivascular clearance and optimizing microvascular health. Lifestyle interventions—especially those that improve sleep[203,204] or use continuous positive airway pressure for obstructive sleep apnea[205]—may augment glymphatic function, while exercise could promote both glymphatic efficiency[206,207] and remyelination.[208,209] Pharmacologically, clemastine has shown remyelination benefits in multiple sclerosis, but extrapolation to WMH/cSVD remains speculative and requires disease-specific trials.[210,211] Moreover, the stronger associations of DWMH with cardiovascular mortality,[171] recurrent stroke,[193,194] and vascular dementia[195,196] suggest that, despite the limitations of CBF measurements alone, DWMH may be more vulnerable under ischemic stress. Maintaining perfusion and vascular reserve may therefore be particularly critical in deep-predominant pathology. For example, isosorbide mononitrate and cilostazol improved white-matter CVR and composite vascular/cognitive outcomes when added to standard care.[212,213] In addition, a randomized trial demonstrated that a Mediterranean-like diet enhanced cerebral perfusion compared with a Western-like diet.[214]

Prognosis and longitudinal monitoring based on temporal heterogeneity

Longitudinal MRI signatures provide prognostic information by delineating the temporal cascade of WMH injury, thereby defining a window for targeted prevention and surveillance. The key is identifying tissue at risk, most evident within the perilesional penumbra. Notably, the hemodynamic penumbra—defined by reduced CBF—is typically broader (~7–14 mm) than the structural penumbra defined by diffusion changes (~2–6 mm),[78,180,181] suggesting that perfusion deficits precede overt tissue injury. This sequence from vascular dysfunction to subsequent structural damage is further supported by evidence that BBB leakage in the penumbra predicts subsequent microstructural decline.[91] However, this cascade does not imply that all axonal or myelin loss in WMH is ischemic in origin. Non-ischemic demyelination can occur independently of vascular insufficiency, as exemplified by autoimmune demyelinating diseases such as multiple sclerosis.[121,124,125,215,216] Non-ischemic demyelination within WMH may present with disproportionate reductions in myelin-sensitive measures despite relatively preserved perfusion, suggesting primary myelin loss rather than secondary ischemic injury. Accordingly, integrating quantitative myelin indices with perfusion metrics could distinguish whether demyelination in a given WMH arises from ischemic injury, primary demyelinating processes, or mixed pathology—thereby enabling a more comprehensive understanding of WMH progression mechanisms.

These vascular and microstructural signatures may assist clinicians in identifying patients on an accelerated trajectory of WMH accumulation. For individuals at high risk based on longitudinal MRI markers, early treatment should target initial pathobiological processes—impaired perfusion and BBB dysfunction—through intervantions such as intensive blood-pressure control[197-199] and pharmacologic enhancement of cerebrovascular function[212,213] before substantial tissue loss ensues. Because total WMH volume evolves slowly and is an insensitive short-term marker, follow-up should emphasize more responsive surrogates, tailored to clinical feasibility. Non-contrast ASL perfusion can detect hemodynamic changes preceding WMH growth.[56,78,176,180-181] and remains valuable for ischemic penumbra assessment in stroke.[209-211] When advanced imaging is unavailable, serial FLAIR at 1–2-year intervals, assessed by visual grading or volumetry, can still differentiate rapid from slow progressors and guide preventive intensity.[217]

Stroke patients with advanced WMH accumulation face higher risks of poor functional outcomes, stroke recurrence, and mortality. Our nationwide multicenter studies demonstrated that higher baseline WMH burden independently worsens outcomes after ischemic stroke,[14,15,218] underscoring its prognostic value for secondary prevention. The detrimental impact of WMH volume is particularly pronounced in mild stroke, where WMH burden strongly predicts 3-month functional outcomes, whereas this association weakens in moderate to severe stroke.[218] Thus, active monitoring and management of WMH progression may

be more important in mild stroke. In addition, although WMH distribution is typically symmetric between hemispheres, we observed that asymmetric WMHs were associated with both old silent and acute lacunar infarcts ipsilateral to the hemisphere with greater WMH burden, supporting the inclusion of WMH asymmetry in clinical risk assessment.[53]

From spatial dichotomy to fine-grained parcellation frameworks

Building on the multimodal and spatially informed insights discussed above, recent advances have begun to move beyond the traditional periventricular–deep (PV–D) dichotomy toward finer parcellation frameworks that capture the full complexity of WMH heterogeneity.[219-222] While the PV–D classification has provided fundamental insights into spatially distinct mechanisms—such as periventricular interstitial edema and deep perforating arteriolar ischemia—emerging evidence indicates that higher spatial resolution can uncover additional mechanistic subtypes with distinct etiologic and prognostic implications.

Our recent work[219] has integrated anatomically meaningful spatial classifications—combining arterial territories[223] and functional lobes[220,221] with concentric distance-from-ventricle layers—into a comprehensive bullseye parcellation framework. Applying machine learning disease-progression models such as Subtype and Stage Inference to FLAIR-based WMH segmentations from large clinical cohorts, this approach identified three distinct spatiotemporal WMH progression patterns: fronto-parietal, radial, and temporo-occipital subtypes. Each subtype exhibits unique associations with demographic factors, vascular risk profiles, stroke etiologies, and clinical outcomes, underscoring that spatial phenotyping can differentiate underlying pathobiology beyond the traditional PV–D dichotomy. These findings highlight that WMH heterogeneity extends beyond simple location-based distinctions; fine-grained spatial mapping reveals mechanistically distinct trajectories, which can be integrated with multimodal MRI signatures to build a more comprehensive model of WMH pathophysiology.

A major barrier to implementing such spatially resolved analyses has been the labor-intensive nature of manual WMH segmentation, especially in large-scale or clinical datasets. Although deep-learning algorithms have markedly improved automation, most were originally optimized for research-grade MRI (slice thickness ~1 mm), limiting performance on the thicker slices (≥5 mm) typical of clinical protocols. Addressing this limitation, we and others recently developed deep-learning algorithms optimized for clinical-grade imaging, demonstrating robust segmentation performance even on thick-slice acquisitions.[45,224] To facilitate broad adoption, we are developing an open-source toolbox that integrates this automated segmentation pipeline with our fine-grained parcellation framework. This resource will support large-scale, mechanism-oriented investigations of WMH heterogeneity across diverse clinical populations and imaging settings, accelerating translation of spatially resolved WMH analytics into both research and clinical practice.

Conclusions

In this review, we integrated multimodal MRI evidence for WMH pathobiology across four complementary axes: (1) WMH versus NAWM, (2) PVWMH versus DWMH, (3) lesion core versus penumbra, and (4) longitudinal progression. Together, these axes provide a mechanistic framework that links diverse MRI signatures to plausible pathobiological subtypes involving microstructural damage, demyelination/macromolecular compromise, BBB leakage and interstitial fluid shifts, hypoperfusion/vascular reactivity failure, and glymphatic-perivascular dysfunction. This approach moves beyond prior summaries by translating lesion patterns into underlying processes and progression pathways, and by highlighting the perilesional penumbra as a dynamic zone of tissue at risk. Future work should validate and extend this MRI-based taxonomy through well-designed longitudinal studies that integrate imaging with histopathology, refine penumbra definitions, and standardize spatial frameworks (including distance-to-ventricle layers and lobe/territory parcellations). Composite biomarkers that combine microstructural damage (e.g., FA/MD/RD/FW), myelin/macromolecular integrity (R1, MTR/MWF, T1w/T2w), vascular integrity and perfusion (K_{trans}/PS/K_i/V_L, CBF/CBV/MTT, CVR), and metabolic measures (MRS metabolites, FDG-PET) are likely to capture tissue vulnerability more effectively than any single metric. Mechanistic targets—particularly glymphatic clearance and CVR—warrant focused investigation given their associations with incident and progressive WMH and their potential modifiability. Finally, fine-grained spatial parcellation and clinical-grade automated segmentation will be essential to extend these insights across diverse cohorts and routine imaging (including thicker-slice clinical FLAIR). Integrating such tools with multimodal MRI can enable mechanism-aware risk stratification, monitoring, and trial design, thereby advancing the field from descriptive lesion mapping toward spatially resolved, pathophysiology-driven precision care for patients with WMH.

Funding statement

This study was supported by grants from the National Priority

https://doi.org/10.5853/jos.2025.04168

Research Center Program (NRF-2021R1A6A1A03038865), the Bio & Medical Technology Development Program (Bioimaging Data Curation Center; RS-2022-NR068424), and the Basic Science Research Program (RS-2025-00514203) of the National Research Foundation funded by the Korean government.

Conflicts of interest

The authors have no financial conflicts of interest.

Author contribution

Conceptualization: Jinyong Chung, Hyerin Oh, Dong-Eog Kim. Study design: Jinyong Chung, Hyerin Oh, Dong-Eog Kim. Methodology: Jinyong Chung, Hyerin Oh, Dong-Eog Kim. Data collection: all authors. Investigation: all authors. Writing—original draft: Jinyong Chung, Dong-Eog Kim. Writing—review & editing: all authors. Funding acquisition: Dong-Eog Kim. Approval of final manuscript: all authors.

References

1. Longstreth WT Jr, Manolio TA, Arnold A, Burke GL, Bryan N, Jungreis CA, et al. Clinical correlates of white matter findings on cranial magnetic resonance imaging of 3301 elderly people: the cardiovascular health study. *Stroke* 1996;27:1274-1282.
2. Wen W, Sachdev PS, Li JJ, Chen X, Anstey KJ. White matter hyperintensities in the forties: their prevalence and topography in an epidemiological sample aged 44-48. *Hum Brain Mapp* 2009;30:1155-1167.
3. de Leeuw FE, de Groot JC, Achten E, Oudkerk M, Ramos LM, Heijboer R, et al. Prevalence of cerebral white matter lesions in elderly people: a population based magnetic resonance imaging study. The Rotterdam scan study. *J Neurol Neurosurg Psychiatry* 2001;70:9-14.
4. Huang WQ, Lin Q, Tzeng CM. Leukoaraiosis: epidemiology, imaging, risk factors, and management of age-related cerebral white matter hyperintensities. *J Stroke* 2024;26:131-163.
5. Das AS, Regenhardt RW, Vernooij MW, Blacker D, Charidimou A, Viswanathan A. Asymptomatic cerebral small vessel disease: insights from population-based studies. *J Stroke* 2019;21:121-138.
6. Ryu WS, Woo SH, Schellingerhout D, Chung MK, Kim CK, Jang MU, et al. Grading and interpretation of white matter hyperintensities using statistical maps. *Stroke* 2014;45:3567-3575.
7. Tosto G, Zimmerman ME, Carmichael OT, Brickman AM; Alzheimer's Disease Neuroimaging Initiative. Predicting aggressive decline in mild cognitive impairment: the importance of white matter hyperintensities. *JAMA Neurol* 2014;71:872-877.
8. Prins ND, Scheltens P. White matter hyperintensities, cognitive impairment and dementia: an update. *Nat Rev Neurol* 2015;11:157-165.
9. Hu HY, Ou YN, Shen XN, Qu Y, Ma YH, Wang ZT, et al. White matter hyperintensities and risks of cognitive impairment and dementia: a systematic review and meta-analysis of 36 prospective studies. *Neurosci Biobehav Rev* 2021;120:16-27.
10. Whitman GT, Tang Y, Lin A, Baloh RW. A prospective study of cerebral white matter abnormalities in older people with gait dysfunction. *Neurology* 2001;57:990-994.
11. Su C, Yang X, Wei S, Zhao R. Association of cerebral small vessel disease with gait and balance disorders. *Front Aging Neurosci* 2022;14:834496.
12. Debette S, Markus HS. The clinical importance of white matter hyperintensities on brain magnetic resonance imaging: systematic review and meta-analysis. *BMJ* 2010;341:c3666.
13. Ghaznawi R, Geerlings MI, Jaarsma-Coes M, Hendrikse J, de Bresser J; UCC-Smart Study Group. Association of white matter hyperintensity markers on MRI and long-term risk of mortality and ischemic stroke: the SMART-MR study. *Neurology* 2021;96:e2172-e2183.
14. Ryu WS, Woo SH, Schellingerhout D, Jang MU, Park KJ, Hong KS, et al. Stroke outcomes are worse with larger leukoaraiosis volumes. *Brain* 2017;140:158-170.
15. Ryu WS, Schellingerhout D, Hong KS, Jeong SW, Jang MU, Park MS, et al. White matter hyperintensity load on stroke recurrence and mortality at 1 year after ischemic stroke. *Neurology* 2019;93:e578-e589.
16. Gouw AA, Seewann A, Vrenken H, van der Flier WM, Rozemuller JM, Barkhof F, et al. Heterogeneity of white matter hyperintensities in Alzheimer's disease: post-mortem quantitative MRI and neuropathology. *Brain* 2008;131(Pt 12):3286-3298.
17. Murray ME, Vemuri P, Preboske GM, Murphy MC, Schweitzer KJ, Parisi JE, et al. A quantitative postmortem MRI design sensitive to white matter hyperintensity differences and their relationship with underlying pathology. *J Neuropathol Exp Neurol* 2012;71:1113-1122.
18. Gouw AA, Seewann A, van der Flier WM, Barkhof F, Rozemuller AM, Scheltens P, et al. Heterogeneity of small vessel disease: a systematic review of MRI and histopathology correlations. *J Neurol Neurosurg Psychiatry* 2011;82:126-135.
19. Fazekas F, Kleinert R, Offenbacher H, Schmidt R, Kleinert G, Payer F, et al. Pathologic correlates of incidental MRI white matter signal hyperintensities. *Neurology* 1993;43:1683-1689.

20. Kim KW, MacFall JR, Payne ME. Classification of white matter lesions on magnetic resonance imaging in elderly persons. *Biol Psychiatry* 2008;64:273-280.
21. Fernando MS, Simpson JE, Matthews F, Brayne C, Lewis CE, Barber R, et al. White matter lesions in an unselected cohort of the elderly: molecular pathology suggests origin from chronic hypoperfusion injury. *Stroke* 2006;37:1391-1398.
22. Simpson JE, Fernando MS, Clark L, Ince PG, Matthews F, Forster G, et al. White matter lesions in an unselected cohort of the elderly: astrocytic, microglial and oligodendrocyte precursor cell responses. *Neuropathol Appl Neurobiol* 2007;33:410-419.
23. Fazekas F, Chawluk JB, Alavi A, Hurtig HI, Zimmerman RA. MR signal abnormalities at 1.5 T in Alzheimer's dementia and normal aging. *AJR Am J Roentgenol* 1987;149:351-356.
24. Scheltens P, Barkhof F, Leys D, Pruvo JP, Nauta JJ, Vermersch P, et al. A semiquantative rating scale for the assessment of signal hyperintensities on magnetic resonance imaging. *J Neurol Sci* 1993;114:7-12.
25. Schmidt R, Fazekas F, Kleinert G, Offenbacher H, Gindl K, Payer F, et al. Magnetic resonance imaging signal hyperintensities in the deep and subcortical white matter. A comparative study between stroke patients and normal volunteers. *Arch Neurol* 1992;49:825-827.
26. Maillard P, Fletcher E, Harvey D, Carmichael O, Reed B, Mungas D, et al. White matter hyperintensity penumbra. *Stroke* 2011;42:1917-1922.
27. Maniega SM, Valdés Hernández MC, Clayden JD, Royle NA, Murray C, Morris Z, et al. White matter hyperintensities and normal-appearing white matter integrity in the aging brain. *Neurobiol Aging* 2015;36:909-918.
28. Wardlaw JM, Makin SJ, Hernández MCV, Armitage PA, Heye AK, Chappell FM, et al. Blood-brain barrier failure as a core mechanism in cerebral small vessel disease and dementia: evidence from a cohort study. *Alzheimers Dement* 2017;13:634-643.
29. Maillard P, Carmichael O, Harvey D, Fletcher E, Reed B, Mungas D, et al. FLAIR and diffusion MRI signals are independent predictors of white matter hyperintensities. *AJNR Am J Neuroradiol* 2013;34:54-61.
30. Etherton MR, Wu O, Cougo P, Giese AK, Cloonan L, Fitzpatrick KM, et al. Integrity of normal-appearing white matter and functional outcomes after acute ischemic stroke. *Neurology* 2017;88:1701-1708.
31. de Groot M, Verhaaren BF, de Boer R, Klein S, Hofman A, van der Lugt A, et al. Changes in normal-appearing white matter precede development of white matter lesions. *Stroke* 2013;44:1037-1042.
32. Zhong G, Lou M. Multimodal imaging findings in normal-appearing white matter of leucoaraiosis: a review. *Stroke Vasc Neurol* 2016;1:59-63.
33. Wardlaw JM, Smith EE, Biessels GJ, Cordonnier C, Fazekas F, Frayne R, et al. Neuroimaging standards for research into small vessel disease and its contribution to ageing and neurodegeneration. *Lancet Neurol* 2013;12:822-838.
34. Cercignani M, Dowell NG, Tofts PS. Quantitative MRI of the brain: principles of physical measurement. 2nd ed. Boca Raton: CRC Press, 2018.
35. Kim KJ, Park M, Joo B, Ahn SJ, Suh SH. Dynamic contrast-enhanced MRI and its applications in various central nervous system diseases. *Investig Magn Reson Imaging* 2022;26:256-264.
36. Henkelman RM, Stanisz GJ, Graham SJ. Magnetization transfer in MRI: a review. *NMR Biomed* 2001;14:57-64.
37. Alsop DC, Detre JA, Golay X, Günther M, Hendrikse J, Hernandez-Garcia L, et al. Recommended implementation of arterial spin-labeled perfusion MRI for clinical applications: a consensus of the ISMRM perfusion study group and the European consortium for ASL in dementia. *Magn Reson Med* 2015;73:102-116.
38. Ross B, Bluml S. Magnetic resonance spectroscopy of the human brain. *Anat Rec* 2001;265:54-84.
39. Schirmer MD, Dalca AV, Sridharan R, Giese AK, Donahue KL, Nardin MJ, et al. White matter hyperintensity quantification in large-scale clinical acute ischemic stroke cohorts – the MRI-GENIE study. *Neuroimage Clin* 2019;23:101884.
40. Kates R, Atkinson D, Brant-Zawadzki M. Fluid-attenuated inversion recovery (FLAIR): clinical prospectus of current and future applications. *Top Magn Reson Imaging* 1996;8:389-396.
41. Fazekas F, Barkhof F, Wahlund LO, Pantoni L, Erkinjuntti T, Scheltens P, et al. CT and MRI rating of white matter lesions. *Cerebrovasc Dis* 2002;13(Suppl 2):31-36.
42. DeCarli C, Fletcher E, Ramey V, Harvey D, Jagust WJ. Anatomical mapping of white matter hyperintensities (WMH): exploring the relationships between periventricular WMH, deep WMH, and total WMH burden. *Stroke* 2005;36:50-55.
43. Kapeller P, Barber R, Vermeulen RJ, Adèr H, Scheltens P, Freidl W, et al. Visual rating of age-related white matter changes on magnetic resonance imaging: scale comparison, interrater agreement, and correlations with quantitative measurements. *Stroke* 2003;34:441-445.
44. Au R, Massaro JM, Wolf PA, Young ME, Beiser A, Seshadri S, et al. Association of white matter hyperintensity volume with decreased cognitive functioning: the Framingham heart study. *Arch Neurol* 2006;63:246-250.
45. Kim H, Ryu WS, Schellingerhout D, Park J, Chung J, Jeong

https://doi.org/10.5853/jos.2025.04168

SW, et al. Automated segmentation of MRI white matter hyperintensities in 8421 patients with acute ischemic stroke. *AJNR Am J Neuroradiol* 2024;45:1885-1894.
46. Kim DE, Park KJ, Schellingerhout D, Jeong SW, Ji MG, Choi WJ, et al. A new image-based stroke registry containing quantitative magnetic resonance imaging data. *Cerebrovasc Dis* 2011;32:567-576.
47. Park G, Hong J, Duffy BA, Lee JM, Kim H. White matter hyperintensities segmentation using the ensemble U-Net with multi-scale highlighting foregrounds. *Neuroimage* 2021;237:118140.
48. Oliveira-Filho J, Ay H, Schaefer PW, Buonanno FS, Chang Y, Gonzalez RG, et al. Diffusion-weighted magnetic resonance imaging identifies the "clinically relevant" small-penetrator infarcts. *Arch Neurol* 2000;57:1009-1014.
49. Calli C, Kitis O, Yunten N. DWI findings of periventricular ischemic changes in patients with leukoaraiosis. *Comput Med Imaging Graph* 2003;27:381-386.
50. Wardlaw JM. Differing risk factors and outcomes in ischemic stroke subtypes: focus on lacunar stroke. *Future Neurol* 2011;6:201-221.
51. Hachinski VC, Potter P, Merskey H. Leuko-araiosis. *Arch Neurol* 1987;44:21-23.
52. Ryu WS, Jeong SW, Kim DE. Total small vessel disease burden and functional outcome in patients with ischemic stroke. *PLoS One* 2020;15:e0242319.
53. Ryu WS, Schellingerhout D, Ahn HS, Park SH, Hong KS, Jeong SW, et al. Hemispheric asymmetry of white matter hyperintensity in association with lacunar infarction. *J Am Heart Assoc* 2018;7:e010653.
54. Griffanti L, Jenkinson M, Suri S, Zsoldos E, Mahmood A, Filippini N, et al. Classification and characterization of periventricular and deep white matter hyperintensities on MRI: a study in older adults. *Neuroimage* 2018;170:174-181.
55. Khan W, Egorova N, Khlif MS, Mito R, Dhollander T, Brodtmann A. Three-tissue compositional analysis reveals in-vivo microstructural heterogeneity of white matter hyperintensities following stroke. *Neuroimage* 2020;218:116869.
56. Thammasart S, Harvey DJ, Maillard P, DeCarli C, Donnay CA, Wheeler GJ, et al. Associations between cerebral blood flow and progression of white matter hyperintensities. *Front Neuroimaging* 2025;3:1463311.
57. Parent O, Bussy A, Devenyi GA, Dai A, Costantino M, Tullo S, et al. Assessment of white matter hyperintensity severity using multimodal magnetic resonance imaging. *Brain Commun* 2023;5:fcad279.
58. Wardlaw JM, Valdés Hernández MC, Muñoz-Maniega S. What are white matter hyperintensities made of? Relevance to vascular cognitive impairment. *J Am Heart Assoc* 2015;4:001140.
59. Madden DJ, Bennett IJ, Song AW. Cerebral white matter integrity and cognitive aging: contributions from diffusion tensor imaging. *Neuropsychol Rev* 2009;19:415-435.
60. Landman BA, Farrell JA, Jones CK, Smith SA, Prince JL, Mori S. Effects of diffusion weighting schemes on the reproducibility of DTI-derived fractional anisotropy, mean diffusivity, and principal eigenvector measurements at 1.5T. *Neuroimage* 2007;36:1123-1138.
61. Bosch B, Arenaza-Urquijo EM, Rami L, Sala-Llonch R, Junqué C, Solé-Padullés C, et al. Multiple DTI index analysis in normal aging, amnestic MCI and AD. Relationship with neuropsychological performance. *Neurobiol Aging* 2012;33:61-74.
62. Nilsson M, van Westen D, Ståhlberg F, Sundgren PC, Lätt J. The role of tissue microstructure and water exchange in biophysical modelling of diffusion in white matter. *MAGMA* 2013;26:345-370.
63. Concha L. A macroscopic view of microstructure: using diffusion-weighted images to infer damage, repair, and plasticity of white matter. *Neuroscience* 2014;276:14-28.
64. Aung WY, Mar S, Benzinger TL. Diffusion tensor MRI as a biomarker in axonal and myelin damage. *Imaging Med* 2013;5:427-440.
65. Seehaus A, Roebroeck A, Bastiani M, Fonseca L, Bratzke H, Lori N, et al. Histological validation of high-resolution DTI in human post mortem tissue. *Front Neuroanat* 2015;9:98.
66. Mancini M, Karakuzu A, Cohen-Adad J, Cercignani M, Nichols TE, Stikov N. An interactive meta-analysis of MRI biomarkers of myelin. *Elife* 2020;9:e61523.
67. Bastin ME, Clayden JD, Pattie A, Gerrish IF, Wardlaw JM, Deary IJ. Diffusion tensor and magnetization transfer MRI measurements of periventricular white matter hyperintensities in old age. *Neurobiol Aging* 2009;30:125-136.
68. Jiaerken Y, Luo X, Yu X, Huang P, Xu X, Zhang M; Alzheimer's Disease Neuroimaging Initiative (ADNI). Microstructural and metabolic changes in the longitudinal progression of white matter hyperintensities. *J Cereb Blood Flow Metab* 2019;39:1613-1622.
69. Promjunyakul NO, Dodge HH, Lahna D, Boespflug EL, Kaye JA, Rooney WD, et al. Baseline NAWM structural integrity and CBF predict periventricular WMH expansion over time. *Neurology* 2018;90:e2119-e2126.
70. Mayer C, Nägele FL, Petersen M, Frey BM, Hanning U, Pasternak O, et al. Free-water diffusion MRI detects structural alterations surrounding white matter hyperintensities in the early stage of cerebral small vessel disease. *J Cereb Blood Flow Metab* 2022;42:1707-1718.
71. Ferris JK, Greeley B, Vavasour IM, Kraeutner SN, Rinat S,

Ramirez J, et al. In vivo myelin imaging and tissue microstructure in white matter hyperintensities and perilesional white matter. *Brain Commun* 2022;4:fcac142.
72. Haddad SMH, Scott CJM, Ozzoude M, Berezuk C, Holmes M, Adamo S, et al. Comparison of diffusion tensor imaging metrics in normal-appearing white matter to cerebrovascular lesions and correlation with cerebrovascular disease risk factors and severity. *Int J Biomed Imaging* 2022;2022:5860364.
73. Etherton MR, Wu O, Giese AK, Rost NS. Normal-appearing white matter microstructural injury is associated with white matter hyperintensity burden in acute ischemic stroke. *Int J Stroke* 2021;16:184-191.
74. Sen PN, Basser PJ. A model for diffusion in white matter in the brain. *Biophys J* 2005;89:2927-2938.
75. Norris DG. The effects of microscopic tissue parameters on the diffusion weighted magnetic resonance imaging experiment. *NMR Biomed* 2001;14:77-93.
76. Budde MD, Xie M, Cross AH, Song SK. Axial diffusivity is the primary correlate of axonal injury in the experimental autoimmune encephalomyelitis spinal cord: a quantitative pixelwise analysis. *J Neurosci* 2009;29:2805-2813.
77. Sidaros A, Engberg AW, Sidaros K, Liptrot MG, Herning M, Petersen P, et al. Diffusion tensor imaging during recovery from severe traumatic brain injury and relation to clinical outcome: a longitudinal study. *Brain* 2008;131(Pt 2):559-572.
78. Wang X, Wang Y, Gao D, Zhao Z, Wang H, Wang S, et al. Characterizing the penumbras of white matter hyperintensities in patients with cerebral small vessel disease. *Jpn J Radiol* 2023;41:928-937.
79. Jensen JH, Helpern JA. MRI quantification of non-Gaussian water diffusion by kurtosis analysis. *NMR Biomed* 2010;23:698-710.
80. Maiter A, Riemer F, Allinson K, Zaccagna F, Crispin-Ortuzar M, Gehrung M, et al. Investigating the relationship between diffusion kurtosis tensor imaging (DKTI) and histology within the normal human brain. *Sci Rep* 2021;11:8857.
81. Falangola MF, Guilfoyle DN, Tabesh A, Hui ES, Nie X, Jensen JH, et al. Histological correlation of diffusional kurtosis and white matter modeling metrics in cuprizone-induced corpus callosum demyelination. *NMR Biomed* 2014;27:948-957.
82. Irie R, Kamagata K, Kerever A, Ueda R, Yokosawa S, Otake Y, et al. The relationship between neurite density measured with confocal microscopy in a cleared mouse brain and metrics obtained from diffusion tensor and diffusion kurtosis imaging. *Magn Reson Med Sci* 2018;17:138-144.
83. Kelm ND, West KL, Carson RP, Gochberg DF, Ess KC, Does MD. Evaluation of diffusion kurtosis imaging in ex vivo hypomyelinated mouse brains. *Neuroimage* 2016;124(Pt A):612-626.
84. Voorter PHM, Stringer MS, van Dinther M, Kerkhofs D, Dewenter A, Blair GW, et al. Heterogeneity and penumbra of white matter hyperintensities in small vessel diseases determined by quantitative MRI. *Stroke* 2025;56:128-137.
85. Di Biase MA, Katabi G, Piontkewitz Y, Cetin-Karayumak S, Weiner I, Pasternak O. Increased extracellular free-water in adult male rats following in utero exposure to maternal immune activation. *Brain Behav Immun* 2020;83:283-287.
86. Le Bihan D, Breton E, Lallemand D, Grenier P, Cabanis E, Laval-Jeantet M. MR imaging of intravoxel incoherent motions: application to diffusion and perfusion in neurologic disorders. *Radiology* 1986;161:401-407.
87. Wong SM, Zhang CE, van Bussel FC, Staals J, Jeukens CR, Hofman PA, et al. Simultaneous investigation of microvasculature and parenchyma in cerebral small vessel disease using intravoxel incoherent motion imaging. *Neuroimage Clin* 2017;14:216-221.
88. Le Bihan D, Breton E, Lallemand D, Aubin ML, Vignaud J, Laval-Jeantet M. Separation of diffusion and perfusion in intravoxel incoherent motion MR imaging. *Radiology* 1988;168:497-505.
89. Fokkinga E, Hernandez-Tamames JA, Ianus A, Nilsson M, Tax CMW, Perez-Lopez R, et al. Advanced diffusion-weighted MRI for cancer microstructure assessment in body imaging, and its relationship with histology. *J Magn Reson Imaging* 2024;60:1278-1304.
90. Sun J, Yu X, Jiaerken Y, Song R, Huang P, Wang C, et al. The relationship between microvasculature in white matter hyperintensities and cognitive function. *Brain Imaging Behav* 2017;11:503-511.
91. Kerkhofs D, Wong SM, Zhang E, Staals J, Jansen JFA, van Oostenbrugge RJ, et al. Baseline blood-brain barrier leakage and longitudinal microstructural tissue damage in the periphery of white matter hyperintensities. *Neurology* 2021;96:e2192-e2200.
92. Wang LL, Williamson BJ, Zhang B, Sriwastawa A, Aziz YN, Antzoulatos E, et al. Microstructural and microvascular features of white matter hyperintensities and their association with small vessel disease markers. *Sci Rep* 2025;15:18567.
93. Powers WJ, Grubb RL Jr, Raichle ME. Physiological responses to focal cerebral ischemia in humans. *Ann Neurol* 1984;16:546-552.
94. Yamaji S, Ishii K, Sasaki M, Imamura T, Kitagaki H, Sakamoto S, et al. Changes in cerebral blood flow and oxygen metabolism related to magnetic resonance imaging white matter hyperintensities in Alzheimer's disease. *J Nucl Med* 1997;38:1471-1474.
95. Brown WR, Thore CR. Review: cerebral microvascular pathol-

https://doi.org/10.5853/jos.2025.04168

ogy in ageing and neurodegeneration. *Neuropathol Appl Neurobiol* 2011;37:56-74.
96. Dhollander T, Raffelt D, Connelly A. Towards interpretation of 3-tissue constrained spherical deconvolution results in pathology. *Proc Intl Soc Mag Reson Med* 2017;25:1815.
97. Khan W, Khlif MS, Mito R, Dhollander T, Brodtmann A. Investigating the microstructural properties of normal-appearing white matter (NAWM) preceding conversion to white matter hyperintensities (WMHs) in stroke survivors. *Neuroimage* 2021;232:117839.
98. Zhang W, Zhou Y, Wang J, Gong X, Chen Z, Zhang X, et al. Glymphatic clearance function in patients with cerebral small vessel disease. *Neuroimage* 2021;238:118257.
99. Taoka T, Masutani Y, Kawai H, Nakane T, Matsuoka K, Yasuno F, et al. Evaluation of glymphatic system activity with the diffusion MR technique: diffusion tensor image analysis along the perivascular space (DTI-ALPS) in Alzheimer's disease cases. *Jpn J Radiol* 2017;35:172-178.
100. Steward CE, Venkatraman VK, Lui E, Malpas CB, Ellis KA, Cyarto EV, et al. Assessment of the DTI-ALPS parameter along the perivascular space in older adults at risk of dementia. *J Neuroimaging* 2021;31:569-578.
101. Taoka T, Ito R, Nakamichi R, Nakane T, Kawai H, Naganawa S. Diffusion tensor image analysis along the perivascular space (DTI-ALPS): revisiting the meaning and significance of the method. *Magn Reson Med Sci* 2024;23:268-290.
102. Wardlaw JM, Benveniste H, Nedergaard M, Zlokovic BV, Mestre H, Lee H, et al. Perivascular spaces in the brain: anatomy, physiology and pathology. *Nat Rev Neurol* 2020;16:137-153.
103. Ramirez J, Berezuk C, McNeely AA, Gao F, McLaurin J, Black SE. Imaging the perivascular space as a potential biomarker of neurovascular and neurodegenerative diseases. *Cell Mol Neurobiol* 2016;36:289-299.
104. Doubal FN, MacLullich AM, Ferguson KJ, Dennis MS, Wardlaw JM. Enlarged perivascular spaces on MRI are a feature of cerebral small vessel disease. *Stroke* 2010;41:450-454.
105. Huang P, Zhang R, Jiaerken Y, Wang S, Yu W, Hong H, et al. Deep white matter hyperintensity is associated with the dilation of perivascular space. *J Cereb Blood Flow Metab* 2021;41:2370-2380.
106. Barnes A, Ballerini L, Valdés Hernández MDC, Chappell FM, Muñoz Maniega S, Meijboom R, et al. Topological relationships between perivascular spaces and progression of white matter hyperintensities: a pilot study in a sample of the Lothian Birth Cohort 1936. *Front Neurol* 2022;13:889884.
107. Jessen NA, Munk AS, Lundgaard I, Nedergaard M. The glymphatic system: a beginner's guide. *Neurochem Res* 2015;40:2583-2599.
108. Marín-Padilla M, Knopman DS. Developmental aspects of the intracerebral microvasculature and perivascular spaces: insights into brain response to late-life diseases. *J Neuropathol Exp Neurol* 2011;70:1060-1069.
109. Iliff JJ, Wang M, Liao Y, Plogg BA, Peng W, Gundersen GA, et al. A paravascular pathway facilitates CSF flow through the brain parenchyma and the clearance of interstitial solutes, including amyloid β. *Sci Transl Med* 2012;4:147ra111.
110. Seiler A, Nöth U, Hok P, Reiländer A, Maiworm M, Baudrexel S, et al. Multiparametric quantitative MRI in neurological diseases. *Front Neurol* 2021;12:640239.
111. Stüber C, Morawski M, Schäfer A, Labadie C, Wähnert M, Leuze C, et al. Myelin and iron concentration in the human brain: a quantitative study of MRI contrast. *Neuroimage* 2014;93(Pt 1):95-106.
112. Rooney WD, Johnson G, Li X, Cohen ER, Kim SG, Ugurbil K, et al. Magnetic field and tissue dependencies of human brain longitudinal 1H2O relaxation in vivo. *Magn Reson Med* 2007;57:308-318.
113. Haast RA, Ivanov D, Formisano E, Uludağ K. Reproducibility and reliability of quantitative and weighted T1 and T2* mapping for myelin-based cortical parcellation at 7 tesla. *Front Neuroanat* 2016;10:112.
114. Storey P, Thompson AA, Carqueville CL, Wood JC, de Freitas RA, Rigsby CK. R2* imaging of transfusional iron burden at 3T and comparison with 1.5T. *J Magn Reson Imaging* 2007;25:540-547.
115. Gelman N, Ewing JR, Gorell JM, Spickler EM, Solomon EG. Interregional variation of longitudinal relaxation rates in human brain at 3.0 T: relation to estimated iron and water contents. *Magn Reson Med* 2001;45:71-79.
116. Langkammer C, Krebs N, Goessler W, Scheurer E, Ebner F, Yen K, et al. Quantitative MR imaging of brain iron: a postmortem validation study. *Radiology* 2010;257:455-462.
117. Warntjes M, Engström M, Tisell A, Lundberg P. Modeling the presence of myelin and edema in the brain based on multiparametric quantitative MRI. *Front Neurol* 2016;7:16.
118. Iordanishvili E, Schall M, Loução R, Zimmermann M, Kotetishvili K, Shah NJ, et al. Quantitative MRI of cerebral white matter hyperintensities: a new approach towards understanding the underlying pathology. *Neuroimage* 2019;202:116077.
119. Park M, Moon Y, Han SH, Kim HK, Moon WJ. Myelin loss in white matter hyperintensities and normal-appearing white matter of cognitively impaired patients: a quantitative synthetic magnetic resonance imaging study. *Eur Radiol* 2019;29:4914-4921.
120. Ganzetti M, Wenderoth N, Mantini D. Whole brain myelin

mapping using T1- and T2-weighted MR imaging data. *Front Hum Neurosci* 2014;8:671.
121. Laule C, Leung E, Lis DK, Traboulsee AL, Paty DW, MacKay AL, et al. Myelin water imaging in multiple sclerosis: quantitative correlations with histopathology. *Mult Scler* 2006;12:747-753.
122. Kozlowski P, Raj D, Liu J, Lam C, Yung AC, Tetzlaff W. Characterizing white matter damage in rat spinal cord with quantitative MRI and histology. *J Neurotrauma* 2008;25:653-676.
123. Laule C, Moore GRW. Myelin water imaging to detect demyelination and remyelination and its validation in pathology. *Brain Pathol* 2018;28:750-764.
124. Tozer D, Ramani A, Barker GJ, Davies GR, Miller DH, Tofts PS. Quantitative magnetization transfer mapping of bound protons in multiple sclerosis. *Magn Reson Med* 2003;50:83-91.
125. Schmierer K, Tozer DJ, Scaravilli F, Altmann DR, Barker GJ, Tofts PS, et al. Quantitative magnetization transfer imaging in postmortem multiple sclerosis brain. *J Magn Reson Imaging* 2007;26:41-51.
126. Lim C, Lee H, Moon Y, Han SH, Kim HJ, Chung HW, et al. Volume and permeability of white matter hyperintensity on cognition: a DCE imaging study of an older cohort with and without cognitive impairment. *J Magn Reson Imaging* 2025;61:2260-2270.
127. Ford JN, Zhang Q, Sweeney EM, Merkler AE, de Leon MJ, Gupta A, et al. Quantitative water permeability mapping of blood-brain-barrier dysfunction in aging. *Front Aging Neurosci* 2022;14:867452.
128. Sourbron SP, Buckley DL. On the scope and interpretation of the Tofts models for DCE-MRI. *Magn Reson Med* 2011;66:735-745.
129. Heye AK, Thrippleton MJ, Armitage PA, Valdés Hernández MDC, Makin SD, Glatz A, et al. Tracer kinetic modelling for DCE-MRI quantification of subtle blood-brain barrier permeability. *Neuroimage* 2016;125:446-455.
130. Tavazzi E, Bergsland N, Kuhle J, Jakimovski D, Ramanathan M, Maceski AM, et al. A multimodal approach to assess the validity of atrophied T2-lesion volume as an MRI marker of disease progression in multiple sclerosis. *J Neurol* 2020;267:802-811.
131. Marstrand JR, Garde E, Rostrup E, Ring P, Rosenbaum S, Mortensen EL, et al. Cerebral perfusion and cerebrovascular reactivity are reduced in white matter hyperintensities. *Stroke* 2002;33:972-976.
132. Bernbaum M, Menon BK, Fick G, Smith EE, Goyal M, Frayne R, et al. Reduced blood flow in normal white matter predicts development of leukoaraiosis. *J Cereb Blood Flow Metab* 2015;35:1610-1615.
133. Zhang R, Huang P, Wang S, Jiaerken Y, Hong H, Zhang Y, et al. Decreased cerebral blood flow and delayed arterial transit are independently associated with white matter hyperintensity. *Front Aging Neurosci* 2022;14:762745.
134. Pantoni L, Garcia JH. Pathogenesis of leukoaraiosis: a review. *Stroke* 1997;28:652-659.
135. Hattori H, Takeda M, Kudo T, Nishimura T, Hashimoto S. Cumulative white matter changes in the gerbil brain under chronic cerebral hypoperfusion. *Acta Neuropathol* 1992;84:437-442.
136. Kudo T, Takeda M, Tanimukai S, Nishimura T. Neuropathologic changes in the gerbil brain after chronic hypoperfusion. *Stroke* 1993;24:259-264; discussion 265.
137. Wakita H, Tomimoto H, Akiguchi I, Kimura J. Glial activation and white matter changes in the rat brain induced by chronic cerebral hypoperfusion: an immunohistochemical study. *Acta Neuropathol* 1994;87:484-492.
138. Shibata M, Ohtani R, Ihara M, Tomimoto H. White matter lesions and glial activation in a novel mouse model of chronic cerebral hypoperfusion. *Stroke* 2004;35:2598-2603.
139. Coltman R, Spain A, Tsenkina Y, Fowler JH, Smith J, Scullion G, et al. Selective white matter pathology induces a specific impairment in spatial working memory. *Neurobiol Aging* 2011;32:2324.e7-2324.e12.
140. Rajeev V, Fann DY, Dinh QN, Kim HA, De Silva TM, Lai MKP, et al. Pathophysiology of blood brain barrier dysfunction during chronic cerebral hypoperfusion in vascular cognitive impairment. *Theranostics* 2022;12:1639-1658.
141. Ishikawa H, Shindo A, Mizutani A, Tomimoto H, Lo EH, Arai K. A brief overview of a mouse model of cerebral hypoperfusion by bilateral carotid artery stenosis. *J Cereb Blood Flow Metab* 2023;43(2_suppl):18-36.
142. Wirestam R, Borg M, Brockstedt S, Lindgren A, Holtås S, Ståhlberg F. Perfusion-related parameters in intravoxel incoherent motion MR imaging compared with CBV and CBF measured by dynamic susceptibility-contrast MR technique. *Acta Radiol* 2001;42:123-128.
143. Kim JS, Lee S, Suh SW, Bae JB, Han JH, Byun S, et al. Association of low blood pressure with white matter hyperintensities in elderly individuals with controlled hypertension. *J Stroke* 2020;22:99-107.
144. Aradi M, Schwarcz A, Perlaki G, Orsi G, Kovács N, Trauninger A, et al. Quantitative MRI studies of chronic brain white matter hyperintensities in migraine patients. *Headache* 2013;53:752-763.
145. Xing Y, Fang F, Zhang X, Hou LL, Zheng ZS, Sheikhali M. Proton magnetic resonance spectroscopy and cognitive impairment in patients with ischemic white matter lesions. *J Res*

https://doi.org/10.5853/jos.2025.04168

Med Sci 2013;18:1061-1066.

146. Erdélyi-Bótor S, Aradi M, Kamson DO, Kovács N, Perlaki G, Orsi G, et al. Changes of migraine-related white matter hyperintensities after 3 years: a longitudinal MRI study. *Headache* 2015;55:55-70.
147. Sappey-Marinier D, Calabrese G, Hetherington HP, Fisher SN, Deicken R, Van Dyke C, et al. Proton magnetic resonance spectroscopy of human brain: applications to normal white matter, chronic infarction, and MRI white matter signal hyperintensities. *Magn Reson Med* 1992;26:313-327.
148. Zhu H, Barker PB. MR spectroscopy and spectroscopic imaging of the brain. In: Modo M, Bulte J. Magnetic resonance neuroimaging: methods and protocols. Totowa: Humana Press, 2010;203-226.
149. Moffett JR, Ross B, Arun P, Madhavarao CN, Namboodiri AM. N-acetylaspartate in the CNS: from neurodiagnostics to neurobiology. *Prog Neurobiol* 2007;81:89-131.
150. Narayana PA. Magnetic resonance spectroscopy in the monitoring of multiple sclerosis. *J Neuroimaging* 2005;15(4 Suppl): 46S-57S.
151. Roschel H, Gualano B, Ostojic SM, Rawson ES. Creatine supplementation and brain health. *Nutrients* 2021;13:586.
152. Pfeuffer J, Tkác I, Provencher SW, Gruetter R. Toward an in vivo neurochemical profile: quantification of 18 metabolites in short-echo-time (1)H NMR spectra of the rat brain. *J Magn Reson* 1999;141:104-120.
153. Dhamala E, Abdelkefi I, Nguyen M, Hennessy TJ, Nadeau H, Near J. Validation of in vivo MRS measures of metabolite concentrations in the human brain. *NMR Biomed* 2019;32: e4058.
154. Basu S, Hess S, Nielsen Braad PE, Olsen BB, Inglev S, Høilund-Carlsen PF. The basic principles of FDG-PET/CT imaging. *PET Clin* 2014;9:355-370.
155. Schöll M, Damián A, Engler H. Fluorodeoxyglucose PET in neurology and psychiatry. *PET Clin* 2014;9:371-390.
156. Simons M, Nave KA. Oligodendrocytes: myelination and axonal support. *Cold Spring Harb Perspect Biol* 2015;8:a020479.
157. Harris JJ, Attwell D. The energetics of CNS white matter. *J Neurosci* 2012;32:356-371.
158. van Swieten JC, van den Hout JH, van Ketel BA, Hijdra A, Wokke JH, van Gijn J. Periventricular lesions in the white matter on magnetic resonance imaging in the elderly: a morphometric correlation with arteriolosclerosis and dilated perivascular spaces. *Brain* 1991;114(Pt 2):761-774.
159. Chimowitz MI, Estes ML, Furlan AJ, Awad IA. Further observations on the pathology of subcortical lesions identified on magnetic resonance imaging. *Arch Neurol* 1992;49:747-752.
160. Keith J, Gao FQ, Noor R, Kiss A, Balasubramaniam G, Au K, et al. Collagenosis of the deep medullary veins: an underrecognized pathologic correlate of white matter hyperintensities and periventricular infarction? *J Neuropathol Exp Neurol* 2017; 76:299-312.
161. Moody DM, Brown WR, Challa VR, Anderson RL. Periventricular venous collagenosis: association with leukoaraiosis. *Radiology* 1995;194:469-476.
162. Fazekas F, Kleinert R, Offenbacher H, Payer F, Schmidt R, Kleinert G, et al. The morphologic correlate of incidental punctate white matter hyperintensities on MR images. *AJNR Am J Neuroradiol* 1991;12:915-921.
163. Munoz DG, Hastak SM, Harper B, Lee D, Hachinski VC. Pathologic correlates of increased signals of the centrum ovale on magnetic resonance imaging. *Arch Neurol* 1993;50:492-497.
164. Thomas AJ, O'Brien JT, Davis S, Ballard C, Barber R, Kalaria RN, et al. Ischemic basis for deep white matter hyperintensities in major depression: a neuropathological study. *Arch Gen Psychiatry* 2002;59:785-792.
165. Min ZG, Shan HR, Xu L, Yuan DH, Sheng XX, Xie WC, et al. Diffusion tensor imaging revealed different pathological processes of white matter hyperintensities. *BMC Neurol* 2021;21: 128.
166. Haller S, Kövari E, Herrmann FR, Cuvinciuc V, Tomm AM, Zulian GB, et al. Do brain T2/FLAIR white matter hyperintensities correspond to myelin loss in normal aging? A radiologic-neuropathologic correlation study. *Acta Neuropathol Commun* 2013;1:14.
167. Cai J, Sun J, Chen H, Chen Y, Zhou Y, Lou M, et al. Different mechanisms in periventricular and deep white matter hyperintensities in old subjects. *Front Aging Neurosci* 2022;14:940538.
168. Jian X, Xu F, Yang M, Zhang M, Yun W. Correlation between enlarged perivascular space and brain white matter hyperintensities in patients with recent small subcortical infarct. *Brain Behav* 2023;13:e3168.
169. Loos CM, Klarenbeek P, van Oostenbrugge RJ, Staals J. Association between perivascular spaces and progression of white matter hyperintensities in lacunar stroke patients. *PLoS One* 2015;10:e0137323.
170. Zou Q, Wang M, Zhang D, Wei X, Li W. White matter hyperintensities in young patients from a neurological outpatient clinic: prevalence, risk factors, and correlation with enlarged perivascular spaces. *J Pers Med* 2023;13:525.
171. Li H, Jacob MA, Cai M, Kessels RPC, Norris DG, Duering M, et al. Perivascular spaces, diffusivity along perivascular spaces, and free water in cerebral small vessel disease. *Neurology* 2024;102:e209306.
172. Spilt A, Goekoop R, Westendorp RG, Blauw GJ, de Craen AJ, van Buchem MA. Not all age-related white matter hyperin-

tensities are the same: a magnetization transfer imaging study. *AJNR Am J Neuroradiol* 2006;27:1964-1968.
173. Todorich B, Pasquini JM, Garcia CI, Paez PM, Connor JR. Oligodendrocytes and myelination: the role of iron. *Glia* 2009;57:467-478.
174. LeVine SM, Macklin WB. Iron-enriched oligodendrocytes: a reexamination of their spatial distribution. *J Neurosci Res* 1990;26:508-512.
175. Anderson VC, Obayashi JT, Kaye JA, Quinn JF, Berryhill P, Riccelli LP, et al. Longitudinal relaxographic imaging of white matter hyperintensities in the elderly. *Fluids Barriers CNS* 2014;11:24.
176. Promjunyakul N, Lahna D, Kaye JA, Dodge HH, Erten-Lyons D, Rooney WD, et al. Characterizing the white matter hyperintensity penumbra with cerebral blood flow measures. *Neuroimage Clin* 2015;8:224-229.
177. Asllani I, Borogovac A, Brown TR. Regression algorithm correcting for partial volume effects in arterial spin labeling MRI. *Magn Reson Med* 2008;60:1362-1371.
178. Mutsaerts HJ, Richard E, Heijtel DF, van Osch MJ, Majoie CB, Nederveen AJ. Gray matter contamination in arterial spin labeling white matter perfusion measurements in patients with dementia. *Neuroimage Clin* 2013;4:139-144.
179. Pohmann R. Accurate, localized quantification of white matter perfusion with single-voxel ASL. *Magn Reson Med* 2010;64:1109-1113.
180. Promjunyakul NO, Lahna DL, Kaye JA, Dodge HH, Erten-Lyons D, Rooney WD, et al. Comparison of cerebral blood flow and structural penumbras in relation to white matter hyperintensities: a multi-modal magnetic resonance imaging study. *J Cereb Blood Flow Metab* 2016;36:1528-1536.
181. Wu X, Ge X, Du J, Wang Y, Sun Y, Han X, et al. Characterizing the penumbras of white matter hyperintensities and their associations with cognitive function in patients with subcortical vascular mild cognitive impairment. *Front Neurol* 2019;10:348.
182. Wong SM, Jansen JFA, Zhang CE, Hoff EI, Staals J, van Oostenbrugge RJ, et al. Blood-brain barrier impairment and hypoperfusion are linked in cerebral small vessel disease. *Neurology* 2019;92:e1669-e1677.
183. Heye AK, Culling RD, Valdés Hernández Mdel C, Thrippleton MJ, Wardlaw JM. Assessment of blood–brain barrier disruption using dynamic contrast-enhanced MRI. A systematic review. *Neuroimage Clin* 2014;6:262-274.
184. Maillard P, Fletcher E, Lockhart SN, Roach AE, Reed B, Mungas D, et al. White matter hyperintensities and their penumbra lie along a continuum of injury in the aging brain. *Stroke* 2014;45:1721-1726.
185. Sam K, Crawley AP, Conklin J, Poublanc J, Sobczyk O, Mandell DM, et al. Development of white matter hyperintensity is preceded by reduced cerebrovascular reactivity. *Ann Neurol* 2016;80:277-285.
186. Makedonov I, Black SE, Macintosh BJ. BOLD fMRI in the white matter as a marker of aging and small vessel disease. *PLoS One* 2013;8:e67652.
187. Logothetis NK, Pfeuffer J. On the nature of the BOLD fMRI contrast mechanism. *Magn Reson Imaging* 2004;22:1517-1531.
188. Golestani AM, Wei LL, Chen JJ. Quantitative mapping of cerebrovascular reactivity using resting-state BOLD fMRI: validation in healthy adults. *Neuroimage* 2016;138:147-163.
189. Bright MG, Murphy K. Reliable quantification of BOLD fMRI cerebrovascular reactivity despite poor breath-hold performance. *Neuroimage* 2013;83:559-568.
190. Spano VR, Mandell DM, Poublanc J, Sam K, Battisti-Charbonney A, Pucci O, et al. CO2 blood oxygen level-dependent MR mapping of cerebrovascular reserve in a clinical population: safety, tolerability, and technical feasibility. *Radiology* 2013;266:592-598.
191. Sam K, Conklin J, Holmes KR, Sobczyk O, Poublanc J, Crawley AP, et al. Impaired dynamic cerebrovascular response to hypercapnia predicts development of white matter hyperintensities. *Neuroimage Clin* 2016;11:796-801.
192. Sabayan B, van der Grond J, Westendorp RG, van Buchem MA, de Craen AJ. Accelerated progression of white matter hyperintensities and subsequent risk of mortality: a 12-year follow-up study. *Neurobiol Aging* 2015;36:2130-2135.
193. Georgakis MK, Duering M, Wardlaw JM, Dichgans M. WMH and long-term outcomes in ischemic stroke: a systematic review and meta-analysis. *Neurology* 2019;92:e1298-e1308.
194. Ren H, Wang D, Wang X, Wu J, Huang J, Jin H, et al. Association between periventricular hyperintensity or deep white matter hyperintensity and outcomes of patients with ischemic stroke. *Front Neurol* 2025;16:1583318.
195. Kim S, Choi SH, Lee YM, Kim MJ, Kim YD, Kim JY, et al. Periventricular white matter hyperintensities and the risk of dementia: a CREDOS study. *Int Psychogeriatr* 2015;27:2069-2077.
196. Smith CD, Johnson ES, Van Eldik LJ, Jicha GA, Schmitt FA, Nelson PT, et al. Peripheral (deep) but not periventricular MRI white matter hyperintensities are increased in clinical vascular dementia compared to Alzheimer's disease. *Brain Behav* 2016;6:e00438.
197. van den Kerkhof M, de Jong JJA, Voorter PHM, Postma AA, Kroon AA, van Oostenbrugge RJ, et al. Blood-brain barrier integrity decreases with higher blood pressure: a 7T DCE-MRI

https://doi.org/10.5853/jos.2025.04168

study. *Hypertension* 2024;81:2162-2172.
198. SPRINT MIND Investigators for the SPRINT Research Group; Nasrallah IM, Pajewski NM, Auchus AP, Chelune G, Cheung AK, Cleveland ML, et al. Association of intensive vs standard blood pressure control with cerebral white matter lesions. *JAMA* 2019;322:524-534.
199. Dufouil C, Chalmers J, Coskun O, Besançon V, Bousser MG, Guillon P, et al. Effects of blood pressure lowering on cerebral white matter hyperintensities in patients with stroke: the PROGRESS (perindopril protection against recurrent stroke study) magnetic resonance imaging substudy. *Circulation* 2005;112:1644-1650.
200. Alperin N, Oliu CJ, Bagci AM, Lee SH, Kovanlikaya I, Adams D, et al. Low-dose acetazolamide reverses periventricular white matter hyperintensities in iNPH. *Neurology* 2014;82:1347-1351.
201. Lee JM, Yan P, Xiao Q, Chen S, Lee KY, Hsu CY, et al. Methylprednisolone protects oligodendrocytes but not neurons after spinal cord injury. *J Neurosci* 2008;28:3141-3149.
202. Stirling DP, Koochesfahani KM, Steeves JD, Tetzlaff W. Minocycline as a neuroprotective agent. *Neuroscientist* 2005;11:308-322.
203. Xie L, Kang H, Xu Q, Chen MJ, Liao Y, Thiyagarajan M, et al. Sleep drives metabolite clearance from the adult brain. *Science* 2013;342:373-377.
204. Vinje V, Zapf B, Ringstad G, Eide PK, Rognes ME, Mardal KA. Human brain solute transport quantified by glymphatic MRI-informed biophysics during sleep and sleep deprivation. *Fluids Barriers CNS* 2023;20:62.
205. Roy B, Nunez A, Aysola RS, Kang DW, Vacas S, Kumar R. Impaired glymphatic system actions in obstructive sleep apnea adults. *Front Neurosci* 2022;16:884234.
206. He XF, Liu DX, Zhang Q, Liang FY, Dai GY, Zeng JS, et al. Voluntary exercise promotes glymphatic clearance of amyloid beta and reduces the activation of astrocytes and microglia in aged mice. *Front Mol Neurosci* 2017;10:144.
207. Yoo RE, Kim JH, Moon HY, Park JY, Cheon S, Shin HS, et al. Long-term physical exercise facilitates putative glymphatic and meningeal lymphatic vessel flow in humans. *Nat Commun* 2025;16:3360.
208. Faulkner ME, Gong Z, Bilgel M, Laporte JP, Guo A, Bae J, et al. Evidence of association between higher cardiorespiratory fitness and higher cerebral myelination in aging. *Proc Natl Acad Sci U S A* 2024;121:e2402813121.
209. Kujawa MJ, Marcinkowska AB, Grzywińska M, Waśkow M, Romanowski A, Szurowska E, et al. Physical activity and the brain myelin content in humans. *Front Cell Neurosci* 2023;17:1198657.
210. Caverzasi E, Papinutto N, Cordano C, Kirkish G, Gundel TJ, Zhu A, et al. MWF of the corpus callosum is a robust measure of remyelination: results from the ReBUILD trial. *Proc Natl Acad Sci U S A* 2023;120:e2217635120.
211. Green AJ, Gelfand JM, Cree BA, Bevan C, Boscardin WJ, Mei F, et al. Clemastine fumarate as a remyelinating therapy for multiple sclerosis (ReBUILD): a randomised, controlled, double-blind, crossover trial. *Lancet* 2017;390:2481-2489.
212. Blair GW, Janssen E, Stringer MS, Thrippleton MJ, Chappell F, Shi Y, et al. Effects of cilostazol and isosorbide mononitrate on cerebral hemodynamics in the LACI-1 randomized controlled trial. *Stroke* 2022;53:29-33.
213. Wardlaw JM, Woodhouse LJ, Mhlanga II, Oatey K, Heye AK, Bamford J, et al. Isosorbide mononitrate and cilostazol treatment in patients with symptomatic cerebral small vessel disease: the lacunar intervention trial-2 (LACI-2) randomized clinical trial. *JAMA Neurol* 2023;80:682-692.
214. Hoscheidt S, Sanderlin AH, Baker LD, Jung Y, Lockhart S, Kellar D, et al. Mediterranean and Western diet effects on Alzheimer's disease biomarkers, cerebral perfusion, and cognition in mid-life: a randomized trial. *Alzheimers Dement* 2022;18:457-468.
215. Gloor M, Andelova M, Gaetano L, Papadopoulou A, Burguet Villena F, Sprenger T, et al. Longitudinal analysis of new multiple sclerosis lesions with magnetization transfer and diffusion tensor imaging. *Eur Radiol* 2024;34:1680-1691.
216. Meijboom R, Wiseman SJ, York EN, Bastin ME, Valdés Hernández MDC, Thrippleton MJ, et al. Rationale and design of the brain magnetic resonance imaging protocol for FutureMS: a longitudinal multi-centre study of newly diagnosed patients with relapsing-remitting multiple sclerosis in Scotland. *Wellcome Open Res* 2022;7:94.
217. Youssef H, Demirer M, Middlebrooks EH, Anisetti B, Meschia JF, Lin MP. Framingham stroke risk profile score and white matter disease progression. *Neurologist* 2024;29:259-264.
218. Gwak DS, Ryu WS, Schellingerhout D, Chung J, Kim HR, Jeong SW, et al. Effects of white matter hyperintensity burden on functional outcome after mild versus moderate-to-severe ischemic stroke. *Sci Rep* 2024;14:22567.
219. Chung J, Park G, Ryu WS, Schellingerhout D, Kim HR, Gwak DS, et al. Distinct spatiotemporal patterns of white matter hyperintensity progression. *Nat Commun* 2025;16:9360.
220. Sudre CH, Gomez Anson B, Davagnanam I, Schmitt A, Mendelson AF, Prados F, et al. Bullseye's representation of cerebral white matter hyperintensities. *J Neuroradiol* 2018;45:114-122.
221. Jiménez-Balado J, Corlier F, Habeck C, Stern Y, Eich T. Effects of white matter hyperintensities distribution and clustering

on late-life cognitive impairment. *Sci Rep* 2022;12:1955.
222. Botz J, Lohner V, Schirmer MD. Spatial patterns of white matter hyperintensities: a systematic review. *Front Aging Neurosci* 2023;15:1165324.
223. Kim DE, Park JH, Schellingerhout D, Ryu WS, Lee SK, Jang MU, et al. Mapping the supratentorial cerebral arterial territories using 1160 large artery infarcts. *JAMA Neurol* 2019;76:72-80.
224. Laso P, Cerri S, Sorby-Adams A, Guo J, Mateen F, Goebl P, et al. Quantifying white matter hyperintensity and brain volumes in heterogeneous clinical and low-field portable MRI. *Proc IEEE Int Symp Biomed Imaging* 2024;2024:1-12.
225. Liao YP, Urayama SI, Isa T, Fukuyama H. Optimal model mapping for intravoxel incoherent motion MRI. *Front Hum Neurosci* 2021;15:617152.
226. Dvorak AV, Kumar D, Zhang J, Gilbert G, Balaji S, Wiley N, et al. The CALIPR framework for highly accelerated myelin water imaging with improved precision and sensitivity. *Sci Adv* 2023;9:eadh9853.
227. Ulas C, Das D, Thrippleton MJ, Valdés Hernández MDC, Armitage PA, Makin SD, et al. Convolutional neural networks for direct inference of pharmacokinetic parameters: application to stroke dynamic contrast-enhanced MRI. *Front Neurol* 2019;9:1147.
228. Kossen T, Madai VI, Mutke MA, Hennemuth A, Hildebrand K, Behland J, et al. Image-to-image generative adversarial networks for synthesizing perfusion parameter maps from DSC-MR images in cerebrovascular disease. *Front Neurol* 2023;13:1051397.

https://doi.org/10.5853/jos.2025.04168